

Asymptotic Methods For PDE Problems In Fluid Mechanics and Related Systems With Strong Localized Perturbations In Two-Dimensional Domains

Michael J. Ward^{*†} and Mary-Catherine Kropinski^{†‡}

^{*} Department of Mathematics University of British Columbia, Vancouver, B.C., Canada

[†] Department of Mathematics, Simon Fraser University, Burnaby, B.C., Canada

1 Introduction

The method of matched asymptotic expansions is a powerful systematic analytical method for asymptotically calculating solutions to singularly perturbed PDE problems. It has been successfully used in a wide variety of applications (cf. Kevorkian and Cole (1993), Lagerstrom (1988), Dyke (1975)). However, there are certain special classes of problems where this method has some apparent limitations.

In particular, for singular perturbation PDE problems leading to infinite logarithmic series in powers of $\nu = -1/\log \varepsilon$, where ε is a small positive parameter, it is well-known that this method may be of only limited practical use in approximating the exact solution accurately. This difficulty stems from the fact that $\nu \rightarrow 0$ very slowly as ε decreases. Therefore, unless many coefficients in the infinite logarithmic series can be obtained analytically, the resulting low order truncation of this series will typically not be very accurate unless ε is very small. Singular perturbation problems involving infinite logarithmic expansions arise in many areas of application in two-dimensional spatial domains including, low Reynolds number fluid flow past bodies of cylindrical cross-section, low Peclet number convection-diffusion problems with localized obstacles, and the calculation of the mean first passage time for Brownian motion in the presence of small traps, etc.

In this article we survey various singularly perturbed PDE problems in two-dimensional spatial domains where hybrid asymptotic-numerical methods have been formulated and implemented to effectively ‘sum’ infinite logarithmic expansions. Some of the problems considered herein directly relate to fluid mechanics, whereas other problems arise in different scientific

contexts. One primary goal of this chapter is to highlight how a common analytical framework can be used to treat a diverse class of problems having strong localized perturbations in two-dimensional domains.

2 Infinite Logarithmic Expansions: Simple Pipe Flow

We first consider the simple model problem of Titcombe and Ward (1999) to illustrate some main ideas for treating PDE problems with infinite logarithmic expansions. We consider steady, incompressible, laminar flow in a straight pipe containing a thin core. Both the pipe and the core have a constant cross-section of arbitrary shape, and thus the problem is two-dimensional. With these assumptions, the pipe flow is unidirectional and the velocity component w in the axial direction satisfies (cf. Ward-Smith (1980))

$$\Delta w = -\beta, \quad \mathbf{x} \in \Omega \setminus \Omega_\varepsilon, \quad (1a)$$

$$w = 0, \quad \mathbf{x} \in \partial\Omega, \quad (1b)$$

$$w = 0, \quad \mathbf{x} \in \partial\Omega_\varepsilon. \quad (1c)$$

Here $\Omega \in \mathbb{R}^2$ is the dimensionless pipe cross-section and Ω_ε is the cross-section of the thin core. We assume that Ω_ε has radius $\mathcal{O}(\varepsilon)$ and that $\Omega_\varepsilon \rightarrow \mathbf{x}_0$ uniformly as $\varepsilon \rightarrow 0$, where $\mathbf{x}_0 \in \Omega$. We denote the scaled subdomain that results from an $\mathcal{O}(\varepsilon^{-1})$ magnification of the length scale of Ω_ε by $\Omega_1 \equiv \varepsilon^{-1}\Omega_\varepsilon$. In (1a), β is defined in terms of the dynamic viscosity μ of the fluid and the constant pressure gradient dp/dz along the channel by $\beta \equiv -\mu^{-1}dp/dz$. In terms of w , the mean flow velocity \bar{w} is defined by

$$\bar{w} \equiv \frac{1}{A_\Omega} \int_{\Omega \setminus \Omega_\varepsilon} w \, d\mathbf{x}. \quad (2)$$

Here A_Ω is the cross-sectional area of the pipe-core geometry. For laminar flow in pipes of non-circular cross-section, with or without cores, the friction coefficient f is expressed in terms of \bar{w} by $f \equiv -L(dp/dz)/(2\rho\bar{w}^2)$ (cf. Ward-Smith (1980)). As a remark, the Reynolds number is defined by $\text{Re} \equiv \bar{w}L\rho/\mu$, where ρ is the density of the fluid. Laminar flow occurs for Reynolds numbers in the approximate range $0 < \text{Re} < 2000$. In the definition of Re , L is a characteristic diameter defined by $L = 4A_\Omega/P_\Omega$, where P_Ω is the wetted perimeter of the pipe and the core.

The asymptotic solution to (1) is constructed in two different regions: an outer region defined at an $\mathcal{O}(1)$ distance from the perturbing core, and an inner region defined in an $\mathcal{O}(\varepsilon)$ neighborhood of the thin core Ω_ε . The

analysis below will show how to calculate the sum of all the logarithmic terms for w in the limit $\varepsilon \rightarrow 0$ of small core radius.

In the outer region we expand the solution to (1) as

$$w(\mathbf{x}; \varepsilon) = W_0(\mathbf{x}; \nu) + \sigma(\varepsilon)W_1(\mathbf{x}; \nu) + \dots. \quad (3)$$

Here $\nu = \mathcal{O}(1/\log \varepsilon)$ is a gauge function to be chosen, and we assume that $\sigma \ll \nu^k$ for any $k > 0$ as $\varepsilon \rightarrow 0$. Thus, W_0 contains all of the logarithmic terms in the expansion. Substituting (3) into (1a) and (1b), and letting $\Omega_\varepsilon \rightarrow \mathbf{x}_0$ as $\varepsilon \rightarrow 0$, we get that W_0 satisfies

$$\Delta W_0 = -\beta, \quad \mathbf{x} \in \Omega \setminus \{\mathbf{x}_0\}, \quad (4a)$$

$$W_0 = 0, \quad \mathbf{x} \in \partial\Omega, \quad (4b)$$

$$W_0 \text{ is singular as } \mathbf{x} \rightarrow \mathbf{x}_0. \quad (4c)$$

The matching of the outer and inner expansions will determine a singularity behavior for W_0 as $\mathbf{x} \rightarrow \mathbf{x}_0$.

In the inner region near Ω_ε we introduce the inner variables

$$\mathbf{y} = \varepsilon^{-1}(\mathbf{x} - \mathbf{x}_0), \quad v(\mathbf{y}; \varepsilon) = W(\mathbf{x}_0 + \varepsilon\mathbf{y}; \varepsilon). \quad (5)$$

If we naively assume that $v = \mathcal{O}(1)$ in the inner region, we obtain the leading-order problem for v that $\Delta_{\mathbf{y}}v = 0$ outside Ω_1 , with $v = 0$ on $\partial\Omega_1$ and $v \rightarrow W_0(\mathbf{x}_0)$ as $|\mathbf{y}| \rightarrow \infty$, where $\Delta_{\mathbf{y}}$ denotes the Laplacian in the \mathbf{y} variable. This far-field condition as $|\mathbf{y}| \rightarrow \infty$ is obtained by matching v to the outer solution. However, in two-dimensions there is no solution to this problem since the Green's function for the Laplacian grows logarithmically at infinity. To overcome this difficulty, we require that $v = \mathcal{O}(\nu)$ in the inner region and we allow v to be logarithmically unbounded as $|\mathbf{y}| \rightarrow \infty$. Therefore, we expand v as

$$v(\mathbf{y}; \varepsilon) = V_0(\mathbf{y}; \nu) + \mu_0(\varepsilon)V_1(\mathbf{y}) + \dots, \quad (6a)$$

where we write V_0 in the form

$$V_0(\mathbf{y}; \nu) = \nu\gamma v_c(\mathbf{y}). \quad (6b)$$

Here $\gamma = \gamma(\nu)$ is a constant to be determined with $\gamma = \mathcal{O}(1)$ as $\nu \rightarrow 0$, and we assume that $\mu_0 \ll \nu^k$ for any $k > 0$ as $\varepsilon \rightarrow 0$. Substituting (5) and (6) into (1a) and (1c), and allowing $v_c(\mathbf{y})$ to grow logarithmically at infinity, we obtain that $v_c(\mathbf{y})$ satisfies

$$\Delta_{\mathbf{y}}v_c = 0, \quad \mathbf{y} \notin \Omega_1; \quad v_c = 0, \quad \mathbf{y} \in \partial\Omega_1, \quad (7a)$$

$$v_c \sim \log |\mathbf{y}|, \quad \text{as } |\mathbf{y}| \rightarrow \infty. \quad (7b)$$

The unique solution to (7) has the following far-field asymptotic behavior:

$$v_c(\mathbf{y}) \sim \log |\mathbf{y}| - \log d + \frac{\mathbf{p} \cdot \mathbf{y}}{|\mathbf{y}|^2} + \dots, \quad \text{as } |\mathbf{y}| \rightarrow \infty. \quad (7c)$$

The constant $d > 0$, called the logarithmic capacitance of Ω_1 , depends on the shape of Ω_1 but not on its orientation. The vector \mathbf{p} is called the dipole vector. Numerical values for d for different shapes of Ω_1 are given in Ransford (1995), and some of these are reproduced in Table 1. A boundary integral method to compute d for arbitrarily-shaped domains Ω_1 is described and implemented in Dijkstra and Hochstenbach (2008).

Table 1. The logarithmic capacitance, or shape-dependent parameter, d , for some cross-sectional shapes of $\Omega_1 = \varepsilon^{-1}\Omega_\varepsilon$.

Shape of $\Omega_1 \equiv \varepsilon^{-1}\Omega_\varepsilon$	Logarithmic Capacitance d
circle, radius a	$d = a$
ellipse, semi-axes a, b	$d = \frac{a+b}{2}$
equilateral triangle, side h	$d = \frac{\sqrt{3}\Gamma(\frac{1}{3})^3 h}{8\pi^2} \approx 0.422h$
isosceles right triangle, short side h	$d = \frac{3^{3/4}\Gamma(\frac{1}{4})^2 h}{2^{7/2}\pi^{3/2}} \approx 0.476h$
square, side h	$d = \frac{\Gamma(\frac{1}{4})^2 h}{4\pi^{3/2}} \approx 0.5902h$

The leading-order matching condition between the inner and outer solutions will determine the constant γ in (6b). Upon writing (7c) in outer variables and substituting into (6b), we get the far-field behavior

$$v(\mathbf{y}; \varepsilon) \sim \gamma\nu [\log |\mathbf{x} - \mathbf{x}_0| - \log(\varepsilon d)] + \dots, \quad \text{as } |\mathbf{y}| \rightarrow \infty. \quad (8)$$

Choosing

$$\nu(\varepsilon) = -1/\log(\varepsilon d), \quad (9)$$

and matching (8) to the outer expansion (3) for W , we obtain the singularity condition for W_0 ,

$$W_0 = \gamma + \gamma\nu \log |\mathbf{x} - \mathbf{x}_0| + o(1), \quad \text{as } \mathbf{x} \rightarrow \mathbf{x}_0. \quad (10)$$

The singularity behavior in (10) specifies both the regular and singular part of a Coulomb singularity. As such, it provides one constraint for the determination of γ . More specifically, the solution to (4) together with (10) must determine γ , since for a singularity condition of the form $W_0 \sim$

$S \log |\mathbf{x} - \mathbf{x}_0| + R$ for an elliptic equation, the constant R is not arbitrary but is determined as a function of S , \mathbf{x}_0 , and Ω .

The solution for W_0 is decomposed as

$$W_0(\mathbf{x}; \nu) = W_{0H}(\mathbf{x}) - 2\pi\gamma\nu G_d(\mathbf{x}; \mathbf{x}_0). \quad (11)$$

Here $W_{0H}(\mathbf{x})$ is the smooth function satisfying the unperturbed problem

$$\Delta W_{0H} = -\beta, \quad \mathbf{x} \in \Omega; \quad W_{0H} = 0, \quad \mathbf{x} \in \partial\Omega. \quad (12)$$

In (11), $G_d(\mathbf{x}; \mathbf{x}_0)$ is the Dirichlet Green's function satisfying

$$\Delta G_d = -\delta(\mathbf{x} - \mathbf{x}_0), \quad \mathbf{x} \in \Omega; \quad G_d = 0, \quad \mathbf{x} \in \partial\Omega, \quad (13a)$$

$$G_d(\mathbf{x}; \mathbf{x}_0) = -\frac{1}{2\pi} \log |\mathbf{x} - \mathbf{x}_0| + R_d(\mathbf{x}_0; \mathbf{x}_0) + o(1), \quad \text{as } \mathbf{x} \rightarrow \mathbf{x}_0. \quad (13b)$$

Here $R_{d00} \equiv R_d(\mathbf{x}_0; \mathbf{x}_0)$ is the regular part of the Dirichlet Green's function $G_d(\mathbf{x}; \mathbf{x}_0)$ at $\mathbf{x} = \mathbf{x}_0$. This regular part is also known as either the self-interaction term or the Robin constant (cf. Bandle and Flucher (1996)).

Upon substituting (13b) into (11) and letting $\mathbf{x} \rightarrow \mathbf{x}_0$, we compare the resulting expression with (10) to obtain that γ is given by

$$\gamma = \frac{W_{0H}(\mathbf{x}_0)}{1 + 2\pi\nu R_{d00}}. \quad (14)$$

Therefore, for this problem, γ is determined as the sum of a geometric series in ν . The range of validity of (14) is limited to values of ε for which $2\pi\nu|R_{d00}| < 1$. This yields,

$$0 < \varepsilon < \varepsilon_c, \quad \varepsilon_c \equiv \frac{1}{d} \exp[2\pi R_{d00}]. \quad (15)$$

We summarize our result as follows:

Principal Result 1: For $\varepsilon \ll 1$, the outer expansion for (1) is

$$w \sim W_0(\mathbf{x}; \nu) = W_{0H}(\mathbf{x}) - \frac{2\pi\nu W_{0H}(\mathbf{x}_0)}{1 + 2\pi\nu R_{d00}} G_d(\mathbf{x}; \mathbf{x}_0), \quad \text{for } |\mathbf{x} - \mathbf{x}_0| = \mathcal{O}(1), \quad (16a)$$

and the inner expansion with $\mathbf{y} = \varepsilon^{-1}(\mathbf{x} - \mathbf{x}_0)$ is

$$w \sim V_0(\mathbf{y}; \nu) = \frac{\nu W_{0H}(\mathbf{x}_0)}{1 + 2\pi\nu R_{d00}} v_c(\mathbf{y}), \quad \text{for } |\mathbf{x} - \mathbf{x}_0| = \mathcal{O}(\varepsilon). \quad (16b)$$

Here $\nu = -1/\log(\varepsilon d)$, d is defined in (7c), $v_c(\mathbf{y})$ satisfies (7), and W_{0H} satisfies the unperturbed problem (12). Also $G_d(\mathbf{x}; \mathbf{x}_0)$ and $R_{d00} \equiv R_d(\mathbf{x}_0; \mathbf{x}_0)$ are the Dirichlet Green's function and its regular part satisfying (13).

This formulation is referred to as a hybrid asymptotic-numerical method since it uses the asymptotic analysis as a means of reducing the original problem (1) with a hole to the simpler asymptotically related problem (4) with singularity behavior (10). This related problem does not have a boundary layer structure and so is easy to solve numerically. The numerics required for the hybrid problem involve the computation of the unperturbed solution W_{0H} and the Dirichlet Green's function $G_d(\mathbf{x}; \mathbf{x}_0)$. In terms of G_d we then identify its regular part $R_d(\mathbf{x}_0; \mathbf{x}_0)$ at the singular point. From the solution to the canonical inner problem (7) we then compute the logarithmic capacitance, d . The result (16a) then shows that the asymptotic solution only depends on the product of εd and not on ε itself. This feature allows for an asymptotic equivalence between holes of different cross-sectional shape, based on an effective ‘radius’ of the cylinder. This equivalence is known as Kaplun’s equivalence principle (cf. Kaplun (1957), Kropinski et al. (1995)).

An advantage of the hybrid method over the traditional method of matched asymptotic expansions is that the hybrid formulation is able to sum the infinite logarithmic series and thereby provide an accurate approximate solution. From another viewpoint, the hybrid problem is much easier to solve numerically than the full singularly perturbed problem (1). For the hybrid method a change of the shape of Ω_1 requires us to only re-calculate the constant d . This simplification does not occur in a full numerical approach.

We now outline how Principal Result 1 can be obtained by a direct summation of a conventional infinite-order logarithmic expansion for the outer solution given in the form

$$W \sim W_{0H}(\mathbf{x}) + \sum_{j=1}^{\infty} \nu^j W_{0j}(\mathbf{x}) + \mu_0(\varepsilon)W_1 + \dots, \quad (17)$$

with $\mu_0(\varepsilon) \ll \nu^k$ for any $k > 0$. By formulating a similar series for the inner solution, we will derive a recursive set of problems for the W_{0j} for $j \geq 0$ from the asymptotic matching of the inner and outer solutions. We will then sum this series to re-derive the result in Principal Result 1.

In the outer region we expand the solution to (1) as in (17). In (17), $\nu = \mathcal{O}(1/\log \varepsilon)$ is a gauge function to be chosen, while the smooth function W_{0H} satisfies the unperturbed problem (12) in the unperturbed domain. By substituting (17) into (1a) and (1b), and letting $\Omega_\varepsilon \rightarrow \mathbf{x}_0$ as $\varepsilon \rightarrow 0$, we

get that W_{0j} for $j \geq 1$ satisfies

$$\Delta W_{0j} = 0, \quad \mathbf{x} \in \Omega \setminus \{\mathbf{x}_0\}, \quad (18a)$$

$$W_{0j} = 0, \quad \mathbf{x} \in \partial\Omega, \quad (18b)$$

$$W_{0j} \text{ is singular as } \mathbf{x} \rightarrow \mathbf{x}_0. \quad (18c)$$

The matching of the outer and inner expansions will determine a singularity behavior for W_{0j} as $\mathbf{x} \rightarrow \mathbf{x}_0$ for each $j \geq 1$.

In the inner region near Ω_ε we introduce the inner variables

$$\mathbf{y} = \varepsilon^{-1}(\mathbf{x} - \mathbf{x}_0), \quad v(\mathbf{y}; \varepsilon) = W(\mathbf{x}_0 + \varepsilon\mathbf{y}; \varepsilon). \quad (19)$$

We then pose the explicit infinite-order logarithmic inner expansion

$$v(\mathbf{y}; \varepsilon) = \sum_{j=0}^{\infty} \gamma_j \nu^{j+1} v_c(\mathbf{y}). \quad (20)$$

Here γ_j are ε -independent coefficients to be determined. Substituting (20) and (1a) and (1c), and allowing $v_c(\mathbf{y})$ to grow logarithmically at infinity, we obtain that $v_c(\mathbf{y})$ satisfies (7) with far-field behavior (7c).

Upon using the far-field behavior (7c) in (20), and writing the resulting expression in terms of the outer variable $\mathbf{x} - \mathbf{x}_0 = \varepsilon\mathbf{y}$, we obtain that

$$v \sim \gamma_0 + \sum_{j=1}^{\infty} \nu^j [\gamma_{j-1} \log |\mathbf{x} - \mathbf{x}_0| + \gamma_j]. \quad (21)$$

The matching condition between the infinite-order outer expansion (17) as $\mathbf{x} \rightarrow \mathbf{x}_0$ and the far-field behavior (21) of the inner expansion is that

$$W_{0H}(\mathbf{x}_0) + \sum_{j=1}^{\infty} \nu^j W_{0j}(\mathbf{x}) \sim \gamma_0 + \sum_{j=1}^{\infty} \nu^j [\gamma_{j-1} \log |\mathbf{x} - \mathbf{x}_0| + \gamma_j]. \quad (22)$$

The leading-order match yields that

$$\gamma_0 = W_{0H}(\mathbf{x}_0). \quad (23)$$

The higher-order matching condition, from (22), shows that the solution W_{0j} to (18) must have the singularity behavior

$$W_{0j} \sim \gamma_{j-1} \log |\mathbf{x} - \mathbf{x}_0| + \gamma_j, \quad \text{as } \mathbf{x} \rightarrow \mathbf{x}_0. \quad (24)$$

The unknown coefficients γ_j for $j \geq 1$, starting with $\gamma_0 = W_{0H}(\mathbf{x}_0)$, are determined recursively from the infinite sequence of problems (18) and (24)

for $j \geq 1$. The explicit solution to (18) with $W_{0j} \sim \gamma_{j-1} \log |\mathbf{x} - \mathbf{x}_0|$ as $\mathbf{x} \rightarrow \mathbf{x}_0$ is given explicitly in terms of $G_d(\mathbf{x}; \mathbf{x}_0)$ of (13) as

$$W_{0j}(\mathbf{x}) = -2\pi\gamma_{j-1}G_d(\mathbf{x}; \mathbf{x}_0). \quad (25)$$

Next, we expand (25) as $\mathbf{x} \rightarrow \mathbf{x}_0$ and compare it with the required singularity structure (24). This yields

$$-2\pi\gamma_{j-1} \left[-\frac{1}{2\pi} \log |\mathbf{x} - \mathbf{x}_0| + R_{d00} \right] \sim \gamma_{j-1} \log |\mathbf{x} - \mathbf{x}_0| + \gamma_j, \quad (26)$$

where $R_{d00} \equiv R_d(\mathbf{x}_0; \mathbf{x}_0)$. By comparing the non-singular parts of (26), we obtain a recursion relation for the γ_j , valid for $j \geq 1$, given by

$$\gamma_j = (-2\pi R_{d00}) \gamma_{j-1}, \quad \gamma_0 = W_{0H}(\mathbf{x}_0), \quad (27)$$

which has the explicit solution

$$\gamma_j = [-2\pi R_{d00}]^j W_{0H}(\mathbf{x}_0), \quad j \geq 0. \quad (28)$$

Finally, to obtain the outer solution we substitute (25) and (28) into (17) to obtain

$$\begin{aligned} w - W_{0H}(\mathbf{x}) &\sim \sum_{j=1}^{\infty} \nu^j (-2\pi\gamma_{j-1}) G_d(\mathbf{x}; \mathbf{x}_0) = -2\pi\nu G_d(\mathbf{x}; \mathbf{x}_0) \sum_{j=0}^{\infty} \nu^j \gamma_j \\ &\sim -2\pi\nu W_{0H}(\mathbf{x}_0) G_d(\mathbf{x}; \mathbf{x}_0) \sum_{j=0}^{\infty} [-2\pi\nu R_{d00}]^j \\ &\sim -\frac{2\pi\nu W_{0H}(\mathbf{x}_0)}{1 + 2\pi\nu R_{d00}} G_d(\mathbf{x}_0; \mathbf{x}_0). \end{aligned} \quad (29a)$$

Equation (29a) agrees with equation (16a) of Principal Result 1. Similarly, upon substituting (28) into the infinite-order inner expansion (20), we obtain

$$v(\mathbf{y}; \varepsilon) = \nu W_{0H}(\mathbf{x}_0) v_c(\mathbf{y}) \sum_{j=0}^{\infty} [-2\pi R_{d00}\nu]^j = \frac{\nu W_{0H}(\mathbf{x}_0)}{1 + 2\pi\nu R_{d00}} v_c(\mathbf{y}), \quad (30)$$

which recovers equation (16b) of Principal Result 1.

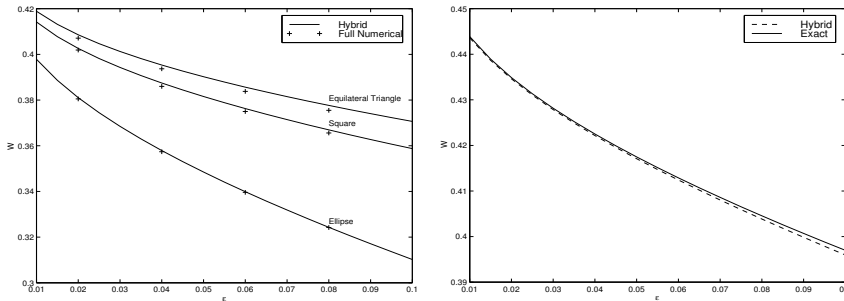
Next, we compare the results of the hybrid method with results obtained either analytically or numerically from the full perturbed problem (1).

We consider flow in a circular pipe Ω of cross-sectional radius r_0 that contains a concentric core Ω_ε of various cross-sectional shapes centered at the origin. We use Table 1 for the logarithmic capacitance d for a square

core, an elliptical core, and an equilateral triangular core. Using the notation in the table, we set the major and minor semi-axes of the ellipse as $a = 2$ and $b = 1$, and both the side of the square and the equilateral triangle as $h = 1$. To compute the hybrid method solution, we readily calculate that the Green's function is $G_d = -(2\pi)^{-1} \log(r/r_0)$ and that the unperturbed solution is $W_{0H} = \beta(r_0^2 - r^2)/4$. The outer hybrid method solution, as obtained from (16a) of Principal Result 1, is simply

$$w(\mathbf{x}; \varepsilon) = \frac{\beta}{4} \left[r_0^2 - r^2 - r_0^2 \frac{\log(r_0/r)}{\log(r_0/[\varepsilon d])} \right], \quad r = |\mathbf{x}|. \quad (31)$$

From (31), we can compute the asymptotic mean flow rate using (2).



(a) Concentric Geometry: \bar{w} vs. ε

(b) Eccentric Geometry: \bar{w} vs. ε

Figure 1. The mean flow velocity \bar{w} versus the cross-sectional ‘radius’ of an inner core pipe located inside a circular pipe of cross-sectional radius $r_0 = 2$. Left figure: (Concentric annulus geometry). Plots of \bar{w} vs. ε for three different cross-sectional shapes of the inner core pipe. The discrete points are the full numerical results. Right figure (Eccentric Geometry). Plots of \bar{w} versus the circular pipe core cross-sectional radius ε when the inner pipe is centered at $\mathbf{x}_0 = (-1, 0)$. The hybrid and exact results are the dotted and solid curves, respectively.

To validate the asymptotic results for \bar{w} , we compare them with corresponding direct numerical results computed from the full problem (1) using the *PDE Toolbox* of MATLAB (1996). For a circular pipe of radius $r_0 = 2$ containing a concentric core and with $\beta = 1$, Fig. 1(a) contains curves of mean flow velocity, \bar{w} , versus ε , a measure of the size of the core, for three

different cross-sectional shapes of the core. In the hybrid method solution, the change in shape and size of the core requires only that we vary the product εd , which allows us to compute the entire ε curve very easily. In contrast, for each change of shape and size of the core in the direct numerical solution, we had to re-create the solution geometry and re-mesh the solution grid when using the *PDE Toolbox* of MATLAB (1996). For a core of elliptic cross-section, the figure shows that the hybrid method results agree very well with those of the direct numerical solution. The slight discrepancy in comparing the results for the other two core cross-sectional shapes, the square and equilateral triangle, could be due to the inability of the numerical method to resolve the non-smooth boundary of the core.

Next, we consider flow in a circular pipe Ω of radius $r_0 > 1$ that contains a circular core Ω_ε of radius ε centered at $\mathbf{x}_0 = (-1, 0)$. For this case, the exact mean flow velocity \bar{w}_E for this eccentric annulus geometry can be written as a complicated infinite series as in Ward-Smith (1980). In contrast, we need only calculate three specific quantities for our hybrid formulation in (16). Firstly, the unperturbed solution is again given by $W_{0H}(r) = \beta(r_0^2 - r^2)/4$. Next, since the inner core cross-section is a circle of radius ε , then the logarithmic capacitance is $d = 1$, so that $\nu = -1/\log \varepsilon$. Finally, using the method of images, we solve (13) analytically to obtain the Green's function

$$G_d(\mathbf{x}; \mathbf{x}_0) = -\frac{1}{2\pi} \log \left(\frac{|\mathbf{x} - \mathbf{x}_0| r_0}{|\mathbf{x} - \mathbf{x}'_0| |\mathbf{x}_0|} \right). \quad (32)$$

Here the image point \mathbf{x}'_0 of \mathbf{x}_0 in the circle of radius r_0 lies along the ray containing \mathbf{x}_0 and satisfies $|\mathbf{x}'_0| |\mathbf{x}_0| = r_0^2$. Comparing (32) with (13b), we can then calculate the self-interaction term as

$$R_{d00} \equiv R_d(\mathbf{x}_0; \mathbf{x}_0) = -\frac{1}{2\pi} \log \left[\frac{r_0}{|\mathbf{x}_0 - \mathbf{x}'_0| |\mathbf{x}_0|} \right]. \quad (33)$$

Substituting (32), (33), $\nu = -1/\log \varepsilon$, and $W_{0H}(r)$, into (16a) we obtain the outer solution for the hybrid method. This solution is then used in (2) with $A_\Omega \sim \pi r_0^2$ to compute the mean flow velocity for the hybrid method. The integral in (2) is obtained from a numerical quadrature. For an eccentric annulus with pipe radius $r_0 = 2$, and with $\beta = 1$, in Fig. 1(b) we plot the mean flow velocity \bar{w} versus the circular core radius ε as obtained from the exact solution and from the hybrid solution. This plot shows that the hybrid method results compare rather well with the exact results.

We remark that for an inner pipe core of an arbitrary shape centered at $\mathbf{x}_0 = (-1, 0)$, the hybrid method solution as obtained above for the eccentric annulus still applies, provided that we replace $\nu = -1/\log \varepsilon$ in (16a) with

$\nu = -1/\log(\varepsilon d)$, where d is to be computed from (7). In particular, if there is an ellipse with semi-axes ε and 2ε centered at $\mathbf{x}_0 = (-1, 0)$ instead of the circle of radius ε , then from Table 1 we get $d = 3/2$. Hence, the plot in Fig. 1(b) for the hybrid solution still applies provided that we replace the horizontal axis in this figure by $3\varepsilon/2$.

3 Some Related Steady-State Problems in Bounded Singularly Perturbed Domains

In this section we extend the analysis of §2 to treat some related steady-state problems. The problem in 3.1, which concerns the distribution of oxygen partial pressure in muscle tissue, involves multiple inclusions in a two-dimensional domain. In §3.2 we show how to extend the method of §2 to a nonlinear problem.

3.1 Oxygen Transport From Capillaries to Skeletal Muscle

The analytical study of tissue oxygenation from capillaries dates from the original work of Krogh (1919). In the oxygen distribution process of the micro-circulation, oxygen binds to its carrier, haemoglobin, in red blood cells, which transports it through the arterioles, branching to the capillary networks, to the collecting venules. In the capillaries, the oxygen is released from its carrier and diffuses into the surrounding tissue. The reviews of Popel (1989), Fletcher (1978), and the references in Titcombe and Ward (2000), provide substantial information on theoretical research in this area.

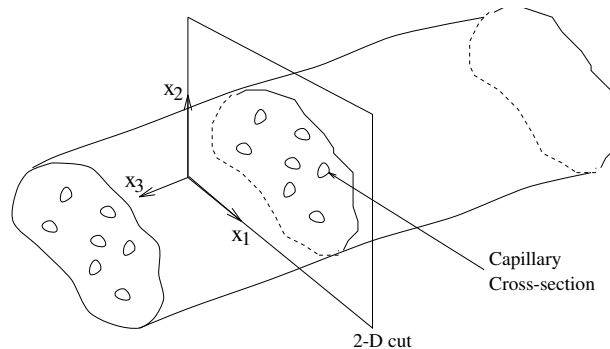


Figure 2. Mathematical idealization of capillary blood supply in skeletal muscle tissue

In this section, we show how to determine the steady-state oxygen partial pressure distribution in a two-dimensional domain representing a transverse section of skeletal muscle tissue that receives oxygen from an array of capillaries of small but arbitrary cross-sectional shape (see Fig. 2). Following the approach of many authors (e.g. Popel (1989)), we model the transport of oxygen from capillaries to tissue by a passive diffusive process. Assuming Fick's law, $J = -D\nabla c$, relating the oxygen flux J to the gradient of oxygen concentration c , and Henry's law, $c = \alpha p$ the dimensionless steady-state oxygen partial pressure p satisfies

$$\Delta p = \mathcal{M}, \quad \mathbf{x} \in \Omega \setminus \Omega_p \quad \Omega_p \equiv \bigcup_{j=1}^N \Omega_{\varepsilon_j}, \quad (34a)$$

$$\partial_n p = 0, \quad \mathbf{x} \in \partial\Omega. \quad (34b)$$

$$\varepsilon \partial_n p + \kappa_j (p - p_{c_j}) = 0, \quad \mathbf{x} \in \partial\Omega_{\varepsilon_j}, \quad j = 1, \dots, N. \quad (34c)$$

The condition (34c) models the capillary wall as a finitely permeable membrane, where $\kappa_i > 0$ is the permeability coefficient of the i^{th} capillary and p_{c_i} is the oxygen partial pressure within the i^{th} capillary (assumed constant). In (34c) and (34b), ∂_n is the outward normal derivative to the tissue domain. In deriving (34) we have assumed that the oxygen diffusivity is spatially constant, and so the oxygen consumption rate \mathcal{M} has been normalized by this constant value. To incorporate skeletal muscle tissue heterogeneities, such as localized oxygen-consuming mitochondria, we assume that \mathcal{M} is spatially-dependent and has the form

$$\mathcal{M}(\mathbf{x}) = \mathcal{M}_0 + \sum_{i=1}^m \mathcal{M}_i \exp\left(-\frac{|\mathbf{x} - \mathbf{x}_i|^2}{\sigma_i^2}\right), \quad (35)$$

for some positive constants \mathcal{M}_0 and \mathcal{M}_i for $i = 1, \dots, m$.

The model (34) is an extension of the well-known Krogh cylinder model Krogh (1919), which consists of one capillary of circular cross-section concentric with a circular cross-section of muscle tissue. For this concentric annulus geometry $\varepsilon < |\mathbf{x}| < 1$, the exact radially symmetric solution p_e is

$$p_e(r) = p_{c1} + \frac{\mathcal{M}}{2} \left[\frac{r^2 - \varepsilon^2}{2} + \frac{\varepsilon^2 - 1}{\kappa_1} + \log\left(\frac{\varepsilon}{r}\right) \right]. \quad (36)$$

This shows that $p_e = \mathcal{O}(\log \varepsilon)$ as $\varepsilon \rightarrow 0$, as induced by the Neumann boundary condition in (34b) on the boundary of the cross-section. In the extended model (34), formulated originally in Titcombe and Ward (2000), one allows for multiple capillaries of arbitrary location, of arbitrary cross-sectional shape, and for the tissue domain to be arbitrary.

Most previous attempts to study the oxygenation of muscle tissue analytically have assumed that the capillaries can be represented as point sources for (34). However, by using the method of matched asymptotic expansions, we show that this type of rough simplification represents only the leading-order term in an infinite asymptotic expansion of the oxygen partial pressure in powers of $-1/\log \varepsilon$, where ε is a measure of the capillary cross-section. From a physiological viewpoint, this type of point-source approximation ignores the effect of the shape of the capillary cross-section and the effect of the interaction between the capillaries. When many capillaries are present, the effect of the capillary interaction should be significant.

Our goal here is to extend the hybrid method of §2 to calculate the asymptotic solution to (34) with an error that is smaller than any power of $-1/\log \varepsilon$. Such an approach, which effectively sums the infinite logarithmic series, takes into account the effect of the capillary interaction.

In the outer region we expand the solution to (34) as

$$p(\mathbf{x}; \varepsilon) = P_0(\mathbf{x}; \nu_1, \dots, \nu_N) + \sigma(\varepsilon)P_1(\mathbf{x}; \nu_1, \dots, \nu_N) + \dots \quad (37)$$

Here $\nu_j = \mathcal{O}(1/\log \varepsilon)$ for $j = 1, \dots, N$ are gauge functions to be chosen, and we assume that $\sigma \ll \nu_j^k$ for any $k > 0$ as $\varepsilon \rightarrow 0$. Thus, P_0 contains all of the logarithmic terms in the expansion. Substituting (37) into (34a) and (34b), and letting $\Omega_{\varepsilon_j} \rightarrow \mathbf{x}_j$ as $\varepsilon \rightarrow 0$, we get that P_0 satisfies

$$\Delta P_0 = \mathcal{M}, \quad \mathbf{x} \in \Omega \setminus \{\mathbf{x}_1, \dots, \mathbf{x}_N\}, \quad (38a)$$

$$\partial_n P_0 = 0, \quad \mathbf{x} \in \partial\Omega, \quad (38b)$$

$$P_0 \text{ is singular as } \mathbf{x} \rightarrow \mathbf{x}_j. \quad (38c)$$

The matching of the outer and inner expansions will determine singularity behaviors for P_0 as $\mathbf{x} \rightarrow \mathbf{x}_j$ for $j = 1, \dots, N$.

In the inner region near the j^{th} capillary Ω_{ε_j} we introduce the inner variables

$$\mathbf{y} = \varepsilon^{-1}(\mathbf{x} - \mathbf{x}_j), \quad p(\mathbf{y}; \varepsilon) = q_j(\mathbf{x}_j + \varepsilon\mathbf{y}; \varepsilon), \quad (39)$$

together with the local expansion

$$q_j = p_{cj} + q_{0j}(\mathbf{y}; \nu_1, \dots, \nu_N) + \mu q_{1j}(\mathbf{y}; \nu_1, \dots, \nu_N) + \dots \quad (40)$$

Here we assume that $\mu \ll \nu_j^k$ for any $k > 0$. We then write q_{0j} in the form

$$q_{0j} = A_j q_{cj}(\mathbf{y}), \quad (41)$$

where $A_j = A_j(\nu_1, \dots, \nu_N)$ is an unknown constant to be determined, and $q_{cj}(\mathbf{y}) \sim \log |\mathbf{y}|$ as $\mathbf{y} \rightarrow \infty$. By substituting (39), (40), and (41), into (34a)

and (34c), we readily derive that q_{cj} is the solution to

$$\Delta_{\mathbf{y}} q_{cj} = 0, \quad \mathbf{y} \notin \Omega_j; \quad \partial_n q_{cj} + \kappa_j q_c = 0, \quad \mathbf{y} \in \partial\Omega_j, \quad (42a)$$

$$q_{cj} \sim \log |\mathbf{y}|, \quad \text{as } |\mathbf{y}| \rightarrow \infty, \quad (42b)$$

where $\Omega_j \equiv \varepsilon^{-1} \Omega_{\varepsilon_j}$. The unique solution to (42) has the following far-field asymptotic behavior:

$$q_{cj}(\mathbf{y}) \sim \log |\mathbf{y}| - \log d_j + \mathcal{O}\left(\frac{1}{|\mathbf{y}|}\right), \quad |\mathbf{y}| \gg 1. \quad (42c)$$

In comparing (42) with (7) for the pipe problem of §2, we observe that here $d_j = d_j(\kappa_j)$. For a particular cross-sectional shape of the capillary and for a given value of κ_j , one must compute $d_j = d_j(\kappa_j)$ numerically from a boundary integral method applied to (42). For a circular capillary of radius ε , for which q_{cj} can be found analytically, we readily calculate that

$$d_j = \exp(-1/\kappa_j). \quad (43)$$

Moreover, by comparing (6b) with (41) we observe that here we have introduced a slight change in the definition of the inner solution. In the analysis below, we will show that $A_j = \mathcal{O}(1)$ as $\varepsilon \rightarrow 0$ in (41), which is a direct consequence of the Neumann boundary condition in (34b).

By using (40) and (42c), we re-write the far-field form for $|\mathbf{y}| \gg 1$ of the inner solution in terms of the outer variables as

$$q_j \sim p_{cj} + A_j \log |\mathbf{x} - \mathbf{x}_j| + \frac{A_j}{\nu_j}. \quad (44a)$$

Here we have introduced the logarithmic gauge function ν_j by

$$\nu_j \equiv -\frac{1}{\log(\varepsilon d_j)}. \quad (44b)$$

The matching condition is that the far-field form (44a) of the inner solution must agree with the near-field behavior of the outer solution for p . Thus, P_0 satisfies (38) subject to the following singularity behavior

$$P_0 \sim p_{cj} + A_j \log |\mathbf{x} - \mathbf{x}_j| + \frac{A_j}{\nu_j}, \quad \text{as } \mathbf{x} \rightarrow \mathbf{x}_j, \quad j = 1, \dots, N. \quad (45)$$

As remarked in §2, we emphasize that the singularity behavior in (45) specifies both the regular and singular part of a Coulomb singularity at each \mathbf{x}_j . As such, the singularity behaviors (45) for $j = 1, \dots, N$ will

provide N equations for the determination of the unknown constants A_j for $j = 1, \dots, N$. By using the divergence theorem, it readily follows that (38), together with (45), has a solution if and only if

$$\sum_{j=1}^N A_j = -\frac{1}{2\pi} \int_{\Omega} \mathcal{M}(\mathbf{x}) d\mathbf{x}. \quad (46)$$

This provides one equation for the determination of A_j for $j = 1, \dots, N$, and shows that $A_j = \mathcal{O}(1)$ as $\varepsilon \rightarrow 0$.

Next, we decompose the solution to (38) and (45) in the form

$$P_0 = P_R(\mathbf{x}) - 2\pi \sum_{i=1}^N A_i G_N(\mathbf{x}; \mathbf{x}_i) + \chi. \quad (47)$$

Here χ is an unknown constant, and $P_R(\mathbf{x})$ is the unique solution of

$$\Delta P_R = \mathcal{M} - \frac{1}{|\Omega|} \int_{\Omega} \mathcal{M}(\mathbf{x}) d\mathbf{x}, \quad \mathbf{x} \in \Omega; \quad \partial_n P_R = 0, \quad \mathbf{x} \in \partial\Omega, \quad (48)$$

with $\int_{\Omega} P_R(\mathbf{x}) d\mathbf{x} = 0$. Here $|\Omega|$ denotes the area of Ω . When \mathcal{M} is a spatially independent, then $P_R = 0$ for each $\mathbf{x} \in \Omega$. In (47), $G_N(\mathbf{x}; \boldsymbol{\xi})$ is the Neumann Green's function, defined as the solution to

$$\Delta G_N = \frac{1}{|\Omega|} - \delta(\mathbf{x} - \boldsymbol{\xi}), \quad \mathbf{x} \in \Omega; \quad \partial_n G_N = 0, \quad \mathbf{x} \in \partial\Omega, \quad (49a)$$

$$G_N(\mathbf{x}; \boldsymbol{\xi}) \sim -\frac{1}{2\pi} \log |\mathbf{x} - \boldsymbol{\xi}| + R_N(\boldsymbol{\xi}; \boldsymbol{\xi}) + o(1), \quad \text{as } \mathbf{x} \rightarrow \boldsymbol{\xi}, \quad (49b)$$

with $\int_{\Omega} G_N(\mathbf{x}; \boldsymbol{\xi}) d\mathbf{x} = 0$. The constant $R_N(\boldsymbol{\xi}; \boldsymbol{\xi})$ is called either the self-interaction term or the regular part of G_N . Since G_N and P_R have zero spatial averages, then χ in (47) is the spatial average of P_0 .

Finally, we expand the solution (47) as $\mathbf{x} \rightarrow \mathbf{x}_j$ and we compare the regular part of the resulting expression with the regular part of the required singularity structure in (45). In this way, we obtain N algebraic equations for the unknowns χ and A_1, \dots, A_N :

$$P_R(\mathbf{x}_j) - 2\pi \left[A_j R_{Njj} + \sum_{\substack{i=1 \\ i \neq j}}^N A_i G_{Nji} \right] + \chi = \frac{A_j}{\nu_j} + p_{cj}, \quad j = 1, \dots, N. \quad (50)$$

Here we have defined $R_{Njj} \equiv R_N(\mathbf{x}_j; \mathbf{x}_j)$ and $G_{Nji} \equiv G_N(\mathbf{x}_j; \mathbf{x}_i)$. The remaining equation relating these unknowns is (46). We summarize our asymptotic construction as follows:

Principal Result 2: For $\varepsilon \rightarrow 0$, the asymptotic solution to (34) near the j^{th} capillary, is

$$p \sim p_{cj} + A_j q_{cj}(\mathbf{y}), \quad \mathbf{y} = \varepsilon^{-1}(\mathbf{x} - \mathbf{x}_j) = \mathcal{O}(1), \quad (51a)$$

where q_{cj} satisfies (42). In the outer region, defined at $\mathcal{O}(1)$ distances from the centers of the capillaries, we have

$$p \sim P_R(\mathbf{x}) - 2\pi \sum_{i=1}^N A_i G_N(\mathbf{x}; \mathbf{x}_i) + \chi. \quad (51b)$$

Here $P_R(\mathbf{x})$ satisfies (48), and G_N is the Neumann Green's function, as defined by (49). The constants A_j for $j = 1, \dots, N$ and χ satisfy the $N + 1$ dimensional linear algebraic system defined by (50) and (46).

To implement the hybrid method, we must compute the Neumann Green's function G_N and its regular part R_N . This can be done explicitly for the unit disk (see equation (4.3) of Kolokolnikov et al. (2005)) and for a rectangle. In particular, upon representing points as complex numbers, we obtain for the unit disk that

$$G_N(\mathbf{x}; \boldsymbol{\xi}) = \frac{1}{2\pi} \left(-\log |\mathbf{x} - \boldsymbol{\xi}| - \log \left| \mathbf{x} |\boldsymbol{\xi}| - \frac{\boldsymbol{\xi}}{|\boldsymbol{\xi}|} \right| + \frac{1}{2} (|\mathbf{x}|^2 + |\boldsymbol{\xi}|^2) - \frac{3}{4} \right), \quad (52a)$$

$$R_N(\boldsymbol{\xi}; \boldsymbol{\xi}) = \frac{1}{2\pi} \left(-\log \left| \boldsymbol{\xi} |\boldsymbol{\xi}| - \frac{\boldsymbol{\xi}}{|\boldsymbol{\xi}|} \right| + |\boldsymbol{\xi}|^2 - \frac{3}{4} \right). \quad (52b)$$

For more general domains, G_N and its regular part can be computed numerically from a boundary integral method (see Pillay et al. (to appear, 2010)). Then, after specifying \mathcal{M} , we can compute the smooth function P_R numerically from (48), and evaluate it at each capillary location \mathbf{x}_j . Finally, the effect of the cross-sectional shape of the capillary and the permeability of the capillary wall enters only into the determination of the shape-dependent parameters d_j to be used in $\nu_j = -1/\log(\varepsilon d_j)$ in (50). This information, required in (50) and (46), represents the numerical part of the hybrid algorithm. The numerical solution to the linear system (50) and (46) then determines the strengths, A_i , of the singularities and the average pressure χ as functions of ε .

As an illustration of the theory, we consider $N = 4$ capillaries of circular cross-section, each of radius ε , located inside a circular tissue domain Ω of unit radius. Therefore, $d_i = 1$ for $i = 1, \dots, 4$. For each fixed j , with $j = 1, 2, 3$, the capillaries are centered at the locations $\mathbf{x}_i^j = j/4 (\cos((2i-1)\pi/4), \sin((2i-1)\pi/4))$ for $i = 1, \dots, 4$ (see Fig. 3(a) for

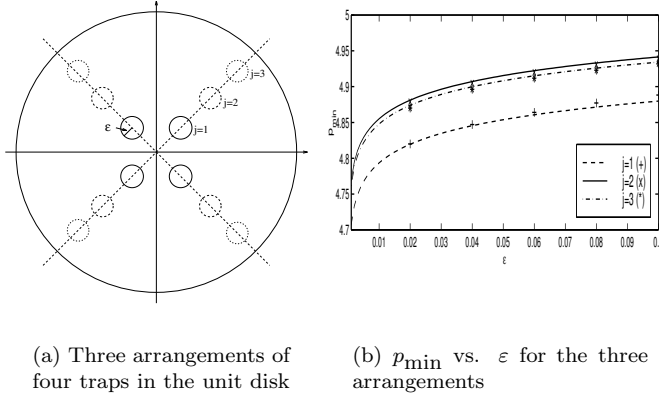


Figure 3. Left figure: Locations of four identical circular capillaries, each of radius ϵ , centered at $(\pm j/4 \cos(\pi/4), \pm j/4 \sin(\pi/4))$ for $j = 1, 2, 3$ inside the unit disk. Right figure: Minimum oxygen partial pressure p_{\min} versus the capillary radius ϵ for the three arrangements shown in the left figure. The parameter values are $\mathcal{M} = 0.3$, with $p_{ci} = 5$ and $\kappa_i = \infty$ for $i = 1, \dots, 4$. The solid curves for $j = 1, 2, 3$ are from the hybrid-method solution, while the discrete points are the full numerical results.

the geometry). For simplicity we choose a constant oxygen consumption rate $\mathcal{M} = 0.3$, with capillary permeability coefficients $\kappa_i = \infty$, and intra-capillary oxygen partial pressure $p_{ci} = 5$, for $i = 1, \dots, 4$. In Fig. 3(b) we plot the minimum oxygen partial pressure $p_{\min} = \min_{\mathbf{x} \in \Omega \setminus \Omega_p} p(\mathbf{x})$ versus ϵ for each of the three arrangements of four traps as calculated from the hybrid formulation (51), (50), and (46). In this figure we also show that the full numerical results for p_{\min} , as computed directly from (34) using the *PDE Toolbox* of MATLAB (1996), agree very well with the hybrid results.

Additional illustrations of the asymptotic theory are given in Titcombe and Ward (2000). It is an open problem to extend the asymptotic methodology to analyze more biologically realistic models of oxygen transport in muscle tissue by considering the local fluid flow inside each capillary and to allow for nonlinear saturation effects on the oxygen consumption rate. More elaborate mathematical models addressing some of these issues are given in Mikelić and Primicerio (2006).

3.2 A Nonlinear Elliptic Problem

Next, we show how the method of §2 can be extended to treat a nonlinear elliptic second-order problem on a bounded two-dimensional domain Ω , which contains a small hole Ω_ε , formulated as

$$\Delta w + F(w) = 0, \quad \mathbf{x} \in \Omega \setminus \Omega_\varepsilon, \quad (53a)$$

$$\partial_n w + b(w - w_b) = 0, \quad \mathbf{x} \in \partial\Omega, \quad (53b)$$

$$w = \alpha, \quad \mathbf{x} \in \partial\Omega_\varepsilon. \quad (53c)$$

Here α is constant, $F(w)$ is a smooth function of w , ∂_n denotes the outward normal derivative, $b > 0$, and Ω_ε is a small hole of radius $\mathcal{O}(\varepsilon)$ with $\Omega_\varepsilon \rightarrow \mathbf{x}_0 \in \Omega$ uniformly as $\varepsilon \rightarrow 0$. Nonlinear problems of this type arise in many applications, including steady-state combustion theory where $F(w)$ is an exponential function (cf. Ward et al. (1993)). The primary difference between the linear problem (1) and the unperturbed problem corresponding to (53) is that, depending on the form of the nonlinearity $F(w)$, the unperturbed problem may have no solution, a unique solution, or multiple solutions. We shall assume that the unperturbed problem has at least one solution, and we will focus on determining how a specific solution to this problem is perturbed by the presence of the subdomain Ω_ε .

In the outer region we expand w as in (3). The leading-order term $W_0(\mathbf{x}; \nu)$ in this expansion satisfies

$$\Delta W_0 + F(W_0) = 0, \quad \mathbf{x} \in \Omega \setminus \{\mathbf{x}_0\}, \quad (54a)$$

$$\partial_n W_0 + b(W_0 - w_b) = 0, \quad \mathbf{x} \in \partial\Omega, \quad (54b)$$

$$W_0 \text{ is singular as } \mathbf{x} \rightarrow \mathbf{x}_0. \quad (54c)$$

The analysis of the solution in the inner region is the same as that in §2 since the effect of the nonlinear term in the inner region is $\mathcal{O}(\varepsilon^2)$, which is transcendentally small compared to the logarithmic terms. Hence, W_0 must have the following singular behavior (see equation (10)):

$$W_0 = \alpha + \gamma + \gamma\nu \log |\mathbf{x} - \mathbf{x}_0| + o(1), \quad \text{as } \mathbf{x} \rightarrow \mathbf{x}_0. \quad (55)$$

Here $\gamma = \gamma(\nu)$ is to be found and ν is defined in terms of the logarithmic capacitance d of (7) by $\nu = -1/\log(\varepsilon d)$.

At this stage, the analysis of (53) differs slightly from its linear counterpart (1). We suppose that for some range of the parameter S we can find a solution to (54) with the singular behavior

$$W_0 \sim S \log |\mathbf{x} - \mathbf{x}_0|, \quad \text{as } \mathbf{x} \rightarrow \mathbf{x}_0. \quad (56)$$

Then, in terms of this solution we define the regular part $R = R(S; \mathbf{x}_0)$ of this Coulomb singularity by

$$R(S; \mathbf{x}_0) = \lim_{\mathbf{x} \rightarrow \mathbf{x}_0} (W_0 - S \log |\mathbf{x} - \mathbf{x}_0|). \quad (57a)$$

In general R is a nonlinear function of S at each \mathbf{x}_0 . Therefore, we have

$$W_0 \sim S \log |\mathbf{x} - \mathbf{x}_0| + R(S; \mathbf{x}_0) + o(1), \quad \text{as } \mathbf{x} \rightarrow \mathbf{x}_0. \quad (57b)$$

By equating (57b) to (55) we get $S = \nu\gamma$ and $R = \alpha + \gamma$, where $\nu = -1/\log(\varepsilon d)$. For fixed εd and α , these relations are two nonlinear algebraic equations for the two unknowns S and γ . Alternatively, we can view these relations as providing a parametric representation of the desired curve $\gamma = \gamma(\nu)$ in the form $\nu = \nu(S)$ and $\gamma = \gamma(S)$, where

$$\gamma = R(S; \mathbf{x}_0) - \alpha, \quad \nu = \frac{S}{R(S; \mathbf{x}_0) - \alpha}. \quad (58)$$

The equation for ν in (58) is an implicit equation determining S in terms of ε from $\nu = -1/\log(\varepsilon d)$. Therefore, we can analytically sum all of the logarithmic terms in the expansion of the solution to (53) provided that we compute the solution to (54), with singular behavior (56), and then identify $R(S; \mathbf{x}_0)$ from (57a). In general this must be done numerically. However, we now illustrate the method with an example where $R(S; \mathbf{x}_0)$ can be calculated analytically.

Let Ω be the unit disk, and take $b = \infty$, $w_b = 0$, $F(w) = e^w$, and assume that Ω_ε is an arbitrarily-shaped hole centered at the origin. Then, (54) and (56) reduce to a radially symmetric problem for $W_0(r)$, given by

$$W_0'' + \frac{1}{r}W_0' + e^{W_0} = 0, \quad 0 < r \leq 1; \quad W_0 = 0, \quad \text{on } r = 1, \quad (59a)$$

$$W_0 \sim S \log r, \quad \text{as } r \rightarrow 0, \quad (59b)$$

where $r = |\mathbf{x}|$. This problem (59) can be solved analytically by first introducing the new variables v and η defined by

$$v = W_0 - S \log r, \quad \eta = r^{1+S/2}. \quad (60)$$

When $S > -2$, we then obtain that $v = v(\eta)$ is smooth and satisfies

$$v'' + \frac{1}{\eta}v' + \left(1 + \frac{S}{2}\right)^{-2} e^v = 0, \quad 0 \leq \eta \leq 1; \quad v = 0, \quad \text{on } \eta = 1. \quad (61)$$

The well-known solution $v = v(\eta)$ to (61) (see Ward et al. (1993)) can be written in parametric form as

$$v(\eta) = 2 \log \left(\frac{1 + \rho}{1 + \rho\eta^2} \right), \quad \left(1 + \frac{S}{2} \right)^{-2} = \frac{8\rho}{(1 + \rho)^2}. \quad (62)$$

The maximum of the right-hand side of the implicit expression for $\rho(S)$ in (62) is 2 and occurs when $\rho = 1$. Therefore, for the existence of a solution to (59) we require that $(1 + S/2)^2 > 1/2$, which yields $S > \sqrt{2} - 2$. When $S > \sqrt{2} - 2$, then $\rho(S)$ from (62) has two roots for ρ , and hence (59) has two solutions. Let us consider the smaller root, labeled by $\rho_-(S)$, given by

$$\rho_-(S) = (S + 1)(S + 3) - (S + 2) [(S + 2)^2 - 2]^{1/2}. \quad (63)$$

Setting $\eta = 0$ in (62), and using (60), we compare with (57a) to obtain

$$v(0) = R(S; 0) = 2 \log(1 + S/2) + \log [8\rho_-(S)]. \quad (64)$$

Substituting (64) into (58) gives a parametric representation of the curve $\gamma = \gamma(\nu)$ in the form $\nu = \nu(S)$ and $\gamma = \gamma(S)$.

4 Slow Viscous Flow Over a Cylinder

Next, we consider the classical problem of slow, steady, two-dimensional flow of a viscous incompressible fluid around an infinitely long straight cylinder. For simplicity, we assume that the cross-sectional shape of the cylinder is symmetric about the direction of the oncoming stream, but otherwise is arbitrary. By slow we mean that the Reynolds number $\varepsilon \equiv U_\infty L/\nu$ is small, where U_∞ is the velocity of the fluid at infinity, ν is the kinematic viscosity, and $2L$ is the diameter of the cross-section of the cylinder.

For $\varepsilon \rightarrow 0$, the method of matched asymptotic expansions was used systematically in Kaplun (1957) and in Proudman and Pearson (1957) to resolve the well-known Stokes paradox, and to calculate asymptotically the stream function in both the Stokes region, which is near the body, and in the Oseen region, which is far from the body. These pioneering studies showed that, for $\varepsilon \rightarrow 0$, the asymptotic expansion for the drag coefficient C_D of a circular cylindrical body starts with $C_D \sim 4\pi\varepsilon^{-1}S(\varepsilon)$, where $S(\varepsilon)$ is an infinite series in powers of $1/\log\varepsilon$. The coefficients in this series are determined in terms of the solutions to certain forced Oseen problems. For a cylinder of arbitrary cross-section, it was shown in Kaplun (1957) that $C_D \sim 4\pi\varepsilon^{-1}S(\varepsilon d_f)$, where d_f is an ‘effective’ radius of the cylinder. This

result establishes a certain asymptotic equivalence for C_D between cylinders of various cross-sectional shapes and is known as Kaplun's equivalence principle.

In an effort to determine C_D quantitatively, analytical formulae for the first three coefficients in $S(\varepsilon)$ were derived in Kaplun (1957). However, as a result of the slow decay of $1/\log \varepsilon$ with decreasing values of ε , the resulting three-term truncated series for C_D agrees rather poorly with the experimental results of Tritton (1959) unless ε is very small. Owing to the complexity of the calculations required, it is impractical to obtain a closer quantitative determination of the drag coefficient by calculating further coefficients in $S(\varepsilon)$ analytically. As a result of these fundamental long-standing difficulties, the problem of slow viscous flow around a cylinder has served as a paradigm for problems where a matched asymptotic analysis fails to be of much practical use, unless ε is very small. A comprehensive recent survey of asymptotic and renormalization group methods applied to slow viscous flow problems is given in Veysey and Goldenfeld (2007).

In Kropinski et al. (1995), this problem was re-examined and a hybrid asymptotic-numerical method was formulated and implemented to effectively sum the infinite logarithmic expansions that arise from the singular perturbation analysis of slow viscous flow around a cylinder. Our approach differs from the hybrid method employed in Lee and Leal (1986) in which numerical methods are used within the framework of the method of matched asymptotic expansions to calculate the first few coefficients in the logarithmic expansions of the flow field and the drag coefficient. Instead, we show that these entire infinite logarithmic series are contained in the solution to a certain related problem that does not involve the cross-sectional shape of the cylinder. The overall framework of our approach is similar to that done in §2 and §3, and is outlined below.

The model formulation is as follows. Consider steady, incompressible, viscous flow around a cylindrical body with a uniform stream of velocity U_∞ in the x direction at large distances from the body. We assume that the cross-section Ω of the cylinder is symmetric with respect to the oncoming stream. Then, in terms of polar coordinates centered inside the body, it follows from the Navier-Stokes equations that the dimensionless stream function ψ satisfies

$$\Delta^2 \psi + \varepsilon J_\rho [\psi, \Delta \psi] = 0, \quad \text{for } \rho > \rho_b(\theta), \quad (65a)$$

$$\psi = \partial_n \psi = 0, \quad \text{on } \rho = \rho_b(\theta), \quad (65b)$$

$$\psi \sim y, \quad \text{as } \rho = (x^2 + y^2)^{1/2} \rightarrow \infty. \quad (65c)$$

Here $\varepsilon \equiv U_\infty L/\nu \ll 1$ is the Reynolds number based on the radius L of

Ω , lengths are in units of L , ∂_n denotes the normal derivative, Δ and Δ^2 denote the Laplacian and Biharmonic operators, respectively, and J_ρ is the Jacobian defined by $J_\rho[a, b] \equiv \rho^{-1}(\partial_\rho a \partial_\theta b - \partial_\theta a \partial_\rho b)$. The boundary of the scaled cross-section is denoted by $\rho = \rho_b(\theta)$ for $-\pi \leq \theta \leq \pi$, and the symmetry condition $\rho_b(\theta) = \rho_b(-\theta)$ is assumed to hold. In terms of ψ , the dimensionless negative vorticity ω is $\omega = \Delta\psi$, and the x and y components of the fluid velocity, u and v , are

$$u = \partial_y \psi = \sin \theta \partial_\rho \psi + \frac{\cos \theta}{\rho} \partial_\theta \psi, \quad v = -\partial_x \psi = -\cos \theta \partial_\rho \psi + \frac{\sin \theta}{\rho} \partial_\theta \psi. \quad (66)$$

We first outline the conventional singular perturbation analysis of (65) for $\varepsilon \rightarrow 0$ (cf. Kaplun (1957) and Proudman and Pearson (1957)). We then formulate the hybrid method for summing the infinite-order logarithmic expansions that arise from the analysis.

In the Stokes, or inner, region defined by $\rho = \mathcal{O}(1)$, the stream function has an infinite logarithmic expansion of the form

$$\psi_s(\rho, \theta) = \sum_{j=1}^{\infty} \nu^j \psi_j(\rho, \theta) + \dots. \quad (67)$$

Here, we define $\nu = \nu(\varepsilon d_f) \equiv -1/\log(\varepsilon d_f e^{1/2})$, where d_f is a shape-parameter that is specified below in terms of the far-field behavior of a Biharmonic problem. For a circular cylinder of radius one then $d_f = 1$. Upon substituting (67) into (65a), we obtain that $\psi_j = a_j \psi_c$, where the a_j for $j \geq 1$ are undetermined constants and $\psi_c \equiv \psi_c(\rho, \theta)$ is the solution to the following canonical inner or Stokes problem:

$$\Delta^2 \psi_c = 0, \quad \text{for } \rho > \rho_b(\theta); \quad \psi_c(\rho, \theta) = -\psi_c(\rho, -\theta), \quad (68a)$$

$$\psi_c = 0 \quad \text{and} \quad \partial_n \psi_c = 0, \quad \text{on } \rho = \rho_b(\theta). \quad (68b)$$

The asymptotic form of ψ_c as $\rho \rightarrow \infty$ involves linear combinations of $\{\rho^3, \rho \log \rho, \rho, \rho^{-1}\} \sin \theta$. However, to match ψ_s with the Oseen expansion below we require that the coefficient of ρ^3 must vanish. Then, to specify ψ_c uniquely, we impose that the coefficient of $\rho \log \rho$ is unity. Therefore, we define ψ_c as the unique solution to (68a) and (68b), with the far-field asymptotic behavior

$$\psi_c \sim \left(\rho \log \rho - \rho \log \left[d_f e^{1/2} \right] \right) \sin \theta, \quad \text{as } \rho \rightarrow \infty. \quad (68c)$$

The constant d_f , depending on the specific shape of the body, is determined uniquely by the solution to (68). This exterior Biharmonic problem (68) is analogous to the exterior Laplace problem (7) for the pipe problem of §2.

Upon substituting $\psi_j = a_j \psi_c$ into (67), the Stokes expansion becomes

$$\psi_s(\rho, \theta) = \sum_{j=1}^{\infty} \nu^j a_j \psi_c(\rho, \theta) + \dots. \quad (69a)$$

Then, by using (68c), we obtain the following far-field behavior of (69a):

$$\psi_s(\rho, \theta) \sim \sum_{j=1}^{\infty} \nu^j a_j \left(\log \rho - \log [d_f e^{1/2}] \right) \rho \sin \theta, \quad \text{as } \rho \rightarrow \infty. \quad (69b)$$

Next, we consider the outer or Oseen region defined for $\rho = \mathcal{O}(\varepsilon^{-1})$. In this region, we introduce the new Oseen, or outer, length-scale r by $r = \varepsilon \rho$ with $r = \mathcal{O}(1)$. We then re-write the far-field behavior of the Stokes solution (69b) in terms of the outer Oseen variable r to obtain

$$\psi_s \sim \frac{1}{\varepsilon} \left(a_1 r \sin \theta + \sum_{j=1}^{\infty} \nu^j [a_j \log r + a_{j+1}] r \sin \theta \right). \quad (69c)$$

This expression (69c) yields a singularity structure for the outer Oseen solution as $r \rightarrow 0$. This behavior suggests that we introduce the new variable Ψ by $\Psi(r, \theta) = \varepsilon \psi(\varepsilon^{-1} r, \theta)$, and that we expand Ψ as

$$\Psi(r, \theta) = r \sin \theta + \nu \Psi_1(r, \theta) + \sum_{j=2}^{\infty} \nu^j \Psi_j(r, \theta) + \dots, \quad (70)$$

in order to satisfy the free-stream condition as $r \rightarrow \infty$ in (65c). Upon substituting (70) into (65a), and matching Ψ as $r \rightarrow 0$ to the required singular behavior (69c), we find that $a_1 = 1$ and that Ψ_1 and Ψ_j , for $j \geq 2$, satisfy the following Oseen problems on $0 < r < \infty$:

$$L_{0s} \Psi_1 \equiv \Delta^2 \Psi_1 + (r^{-1} \sin \theta \partial_\theta - \cos \theta \partial_r) \Delta \Psi_1 = 0, \quad (71a)$$

$$\Psi_1 \sim (\log r + a_2) r \sin \theta, \quad \text{as } r \rightarrow 0; \quad \partial_r \Psi_1 \rightarrow 0, \quad \text{as } r \rightarrow \infty, \quad (71b)$$

$$L_{0s} \Psi_j = - \sum_{k=1}^{j-1} J_r [\Psi_k, \Delta \Psi_{j-k}], \quad (71c)$$

$$\Psi_j \sim (a_j \log r + a_{j+1}) r \sin \theta, \quad \text{as } r \rightarrow 0; \quad \partial_r \Psi_j \rightarrow 0, \quad \text{as } r \rightarrow \infty. \quad (71d)$$

Here L_{0s} is referred to as the linearized Oseen operator, and Ψ_1 is the linearized Oseen solution.

The limiting conditions (71b) and (71d) are the required singularity behaviors of Ψ_1 and Ψ_j for $j \geq 2$, respectively, as $r \rightarrow 0$. For (71b) the strength of the singular part $r \log r \sin \theta$ is set to unity. In terms of the solution to (71a) with $\Psi_1 \sim r \log r \sin \theta$ as $r \rightarrow 0$, we then calculate the constant a_2 of the regular part of the singularity structure from the limiting process $\Psi_1 - r \log r \sin \theta \sim a_2 r \sin \theta$ as $r \rightarrow 0$. Then, with a_2 determined in this way, we solve for Ψ_2 from (71c) with singular behavior $\Psi_2 \sim a_2 r \log r \sin \theta$ as $r \rightarrow 0$. The constant a_3 in the regular part of (71d) is then determined from the limiting process $\Psi_2 - a_2 r \log r \sin \theta \sim a_3 r \sin \theta$ as $r \rightarrow 0$.

Hence, the coefficients a_j for $j = 2, 3, \dots$, which are independent of ε and of the shape of the body, are determined recursively from (71), in a similar way as in §2. The first two coefficients are (cf. Kaplun (1957), Proudman and Pearson (1957))

$$a_2 = \gamma_e - \log 4 - 1 \approx -1.8091, \quad (72a)$$

$$a_3 - a_2^2 = - \int_0^\infty [r^{-1} I_1(2r) + 1 - 4K_1(r)I_1(r)] K_0(r)K_1(r) dr \approx -0.8669. \quad (72b)$$

Here K_1 , K_0 , I_0 and I_1 are the usual modified Bessel functions, and γ_e is Euler's constant. This formula for a_2 was obtained in Kaplun (1957) and Proudman and Pearson (1957), while the expression for a_3 was given in Kaplun (1957). The expression for a_2 was obtained in Proudman and Pearson (1957) in terms of the explicit solution to (71a) with singular behavior $\Psi_1 \sim r \log r \sin \theta$ as $r \rightarrow 0$ given by

$$\Psi_1(r, \theta) = - \sum_{n=1}^{\infty} \frac{c_n(r/2)}{n} r \sin(n\theta), \quad c_n(s) \equiv 2 [K_1(s)I_n(s) + K_0(s)I_n'(s)]. \quad (73)$$

As $r \rightarrow 0$, then $c_n(r/2) = \mathcal{O}(r^{n-1})$ for $n > 1$, and $c_1(r/2) \sim 1 - \log(\rho/4) - \gamma_e$, where γ_e is Euler's constant. Therefore, we conclude that $\Psi_1 - r \log r \sin \theta \rightarrow r(\gamma_e - \log 4 - 1) \sin \theta$ as $r \rightarrow 0$. Hence, from the regular part in (71b), we obtain that $a_2 = \gamma_e - \log 4 - 1$. In contrast, the derivation in Kaplun (1957) of the explicit formula for a_3 given in (72b) is considerably more involved. Explicit analytical formulae for a_j when $j \geq 4$ are not available.

A formula for the drag coefficient C_D is given in Imai (1951) in terms of an arbitrary closed contour around the body. From this formula, and from

the symmetry of the flow, it follows that

$$C_D = \rho \int_0^\pi \left[\cos \theta \left(\psi_\rho^2 - \frac{1}{\rho^2} \psi_\theta^2 \right) - \frac{2}{\rho} \sin \theta \psi_\rho \psi_\theta \right] d\theta - 2\rho \int_0^\pi \omega \psi_\theta \sin \theta d\theta - 2\varepsilon^{-1} \rho \int_0^\pi (\rho\omega_\rho - \omega) \sin \theta d\theta, \quad (74)$$

where ψ satisfies (65) and $\omega = \Delta\psi$. Here ρ , in terms of the Stokes length-scale, is the radius of an arbitrary circular contour that encloses the body. To derive an asymptotic formula for the drag coefficient, we substitute the far-field form (69b) into (74) and evaluate the resulting expression on a large circle $\rho = \rho_0 \gg 1$. In this way, we obtain for $\varepsilon \rightarrow 0$ that the drag coefficient C_D for a cylinder of arbitrary cross-section is given in terms of the coefficients a_j by

$$C_D \sim 4\pi\varepsilon^{-1} \nu(\varepsilon d_f) \left(\sum_{j=0}^{\infty} a_{j+1} \nu^j(\varepsilon d_f) + \dots \right), \quad \nu(\varepsilon d_f) \equiv -\frac{1}{\log[\varepsilon d_f e^{1/2}]}. \quad (75)$$

Kaplun's (see Kaplun (1957)) approximation for C_D results from substituting $a_1 = 1$ and (72) for a_2 and a_3 into (75). The resulting three-term expansion, in equivalent asymptotic form, is

$$C_D \sim \frac{4\pi}{\varepsilon} \hat{\nu}(\varepsilon d_f) [1 - 0.8669 \hat{\nu}^2(\varepsilon d_f)], \quad \hat{\nu}(z) \equiv [\log(3.7027/z)]^{-1}. \quad (76)$$

For a circular cylinder, the explicit form (76) provides a rather poor determination of the experimental drag coefficient unless ε is rather small (cf. Dyke (1975)). One way to overcome this difficulty would be to compute numerically further coefficients a_j , for $j \geq 4$, from the infinite sequence of PDE's (71c) with singularity structures (71d). This would still require truncating the series (75) at some finite j . As an alternative to series truncation, we now follow Kropinski et al. (1995) and formulate a hybrid asymptotic-numerical method that has the effect of summing all the terms on the right-hand side of (75), but which avoids computing the coefficients a_j for $j \geq 1$ individually.

To do so, we let $A^*(z)$ denote a function that is asymptotic to the sum of the terms written explicitly in the brackets on the right-hand side of (75):

$$A^*(z) \sim \sum_{j=1}^{\infty} \nu^{j-1}(z) a_j, \quad z \equiv \varepsilon d_f. \quad (77)$$

Then, the Stokes expansion (69a) is asymptotic to

$$\psi_s(\rho, \theta) = \nu(z)A^*(z)\psi_c(\rho, \theta) + \dots, \quad z = \varepsilon d_f. \quad (78)$$

Substituting (68c) into (78), and writing the resulting expression in terms of the Oseen variable $r = \varepsilon\rho$, we obtain the far-field form in the Stokes region,

$$\psi_s \sim \varepsilon^{-1} A^*(z) [1 + \nu(z) \log r] r \sin \theta. \quad (79)$$

This expression yields the singularity structure for the outer solution.

In the Oseen, or outer region, we do not expand the solution in powers of ν as in (70). Instead, we solve the full problem (65a) and (65c) for $r > 0$ subject to the singularity structure (79), which is to hold as $r \rightarrow 0$. Therefore, in analogy with the approach used in §3.2 (see equations (54)–(58) of §3.2) to treat nonlinear elliptic problems in perforated domains, we introduce the parameter-dependent auxiliary streamfunction $\Psi_H \equiv \Psi_H(r, \theta; S)$, with $\Psi_H(r, \theta; S) = -\Psi_H(r, -\theta; S)$, satisfying

$$\Delta^2 \Psi_H + J_r [\Psi_H, \Delta \Psi_H] = 0, \quad r > 0, \quad (80a)$$

$$\Psi_H \sim r \sin \theta, \quad \text{as } r \rightarrow \infty, \quad (80b)$$

$$\Psi_H \sim Sr \log r \sin \theta, \quad \text{as } r \rightarrow 0. \quad (80c)$$

In Kropinski et al. (1995) (see also Keller and Ward (1996)), this parameter-dependent problem is solved numerically for a range of S values, and in terms of this solution we identify the regular part $R = R(S)$ of this singularity structure by the following limiting process

$$\Psi_H - Sr \log r \sin \theta = R(S)r \sin \theta + o(r), \quad \text{as } r \rightarrow 0. \quad (81)$$

A plot of the numerically computed function $R = R(S)$ is shown in Fig. 4. Given that the hybrid problem (80) is posed on $0 < r < \infty$, it is an interesting open problem to investigate whether it is possible to find an exact solution of (80), in a similar way as was found in (59)–(64) for the nonlinear elliptic problem of §3.2. In this regard, the class of exact solutions to the full 2-D incompressible Navier-Stokes equations found in Ranger (1995) may be useful.

Finally, since the required singularity behavior from (79) is that

$$\Psi_H = A^* [1 + \nu(z) \log r] r \sin \theta + o(r), \quad \text{as } r \rightarrow 0, \quad (82)$$

we conclude that $A^*(z)$ and $\nu(z)$, with $z \equiv \varepsilon d_f$, are given parametrically in terms of the singularity strength S and its regular part $R(S)$ by

$$\nu(z) = -\frac{1}{\log [ze^{1/2}]} = \frac{S}{R(S)}, \quad A^*(z) = R(S). \quad (83)$$

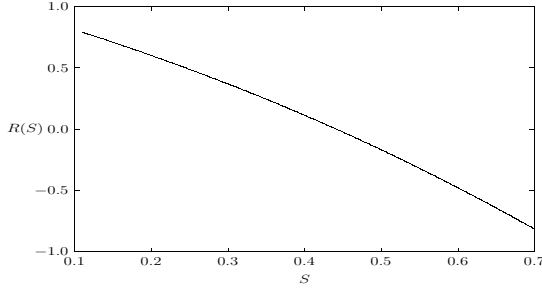


Figure 4. Plot of $R = R(S)$ computed numerically from the hybrid formulation (80) and (81).

The problem (80) is a hybrid asymptotic-numerical formulation of the full problem (65). More specifically, the cylinder in (65) is replaced by the singularity structure (82) that was derived by exploiting the far-field form of the infinite-order logarithmic expansion in the Stokes region. Instead of having to compute solutions to the infinite sequence of problems (71), the hybrid method requires the solution of the parameter-dependent problem (80), with singular behavior (80c) given in terms of the parameter S . Then, the regular part $R = R(S)$ of this singularity behavior is calculated from (81). Finally, (83) determines $A^*(z)$ in terms of $z = \varepsilon d_f$ implicitly.

In terms of A^* and d_f , the asymptotic formula for the drag coefficient, valid to within all logarithmic correction terms, is given by

$$C_D = \frac{4\pi}{\varepsilon} [\nu(z)A^*(z) + \dots], \quad \nu(z) = \frac{-1}{\log [z e^{1/2}]}, \quad z = \varepsilon d_f. \quad (84)$$

Kaplan's equivalence principle follows from the fact that the curve $A^*(z)$ versus z can be used for a cylinder of arbitrary cross-section. To determine $A^*(\varepsilon d_f)$ for a body of a specific shape, we need only compute the single constant d_f from the numerical solution to the canonical Stokes problem (68). This feature provides a significant advantage over a direct numerical approach on the full problem (65).

For a few simple cross-sectional shapes, the constant d_f can be determined analytically from (68). In particular, for a circular cross-section,

where $\rho_b(\theta) = 1$, then the solution to (68) is

$$\psi_c = \left(\rho \log \rho - \frac{\rho}{2} + \frac{1}{2\rho} \right) \sin \theta, \quad (85)$$

so that $d_f = 1$. Next we consider an elliptical domain defined by $(x/a)^2 + (y/b)^2 = 1$ where $\max(a, b) = 1$. In the case where $a = 1$, for which the major axis is aligned parallel to the oncoming stream, the solution to (68) can be found by introducing elliptic cylinder coordinates (see Kropinski et al. (1995)). In this way, we obtain that

$$d_f = \left(\frac{a+b}{2} \right) \exp \left[\frac{b-a}{2(b+a)} \right]. \quad (86)$$

This formula for d_f also holds for the case when $b = 1$ (the major axis is aligned perpendicular to the oncoming stream). A plot of d_f for various ellipses is shown in Fig. 5.

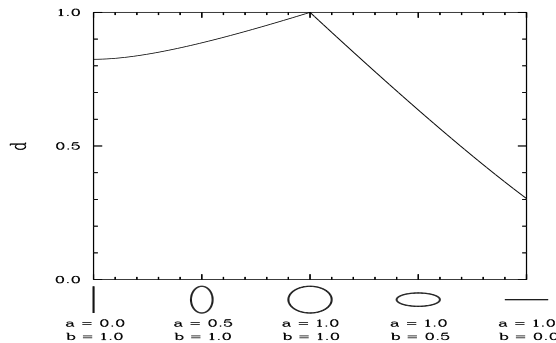


Figure 5. The shape-parameter d_f of (86) for an ellipse with a semi-major axis of unity.

In Kropinski et al. (1995) a numerical conformal mapping method was used to calculate d_f numerically from (68) for other simple cross-sectional shapes that can be mapped to the unit disk. In particular, such an analytical conformal mapping is known for the family of symmetric Karman-Trefftz (KT) airfoils (cf. Milne-Thomson (1958)). The mapping function, $z = z(\sigma)$, for the boundary of these profiles is

$$z(\sigma) = \beta_0 k c \left[\frac{(\xi + c)^k + (\xi - c)^k}{(\xi + c)^k - (\xi - c)^k} \right], \quad \xi \equiv \sigma^{-1} + c - 1, \quad (87a)$$

Table 2. Numerical values for d_f corresponding to the KT airfoils (87). The tail angle (in degrees) is θ_T , and the thickness ratio is δ . The last column gives the value of b for an ellipse, with $a = 1$, that has the same value of d_f as the corresponding airfoil.

δ	θ_T	k	c	d_f	b
.050	0°	2.000	0.961	0.328	0.040
.080	5°	1.972	0.952	0.344	0.066
.100	13°	1.928	0.960	0.354	0.082
.120	16°	1.910	0.954	0.364	0.098
.120	20°	1.889	0.968	0.363	0.096
.200	25°	1.861	0.915	0.410	0.170

where $\sigma = e^{i\theta}$ with $0 \leq \theta \leq 2\pi$. By fixing the length of the airfoil to be 2, we find that the mapping constant β_0 is given in terms of k and c by

$$\beta_0 = \frac{[1 - (1 - c)^k]}{kc}. \quad (87b)$$

A parametric representation for the airfoil profile is obtained by setting $\sigma = e^{i\theta}$ in (87a). In (87), the parameters k and c , where $1 < k < 2$ and $0 < c < 1$, determine the thickness ratio δ of the airfoil and the tail angle θ_T , given by $\theta_T = (2 - k)\pi$. Numerical values for d_f for some KT airfoils, as computed in Kropinski et al. (1995), are given in Table 2.

For each of the KT airfoil examples given in Table 2 there is an equivalent ellipse with $a = 1$ that has the same value of d_f . The values of b for these equivalent ellipses, which are computed using (86), are given in the last column of Table 2. By Kaplun's equivalence principle each of these equivalent ellipses has the same asymptotic drag coefficient, to within all logarithmic correction terms, as the corresponding KT airfoil. However, it is clear that the transcendently small terms in the expansion of the drag coefficient, which are smaller than any power of ν , will not satisfy the same equivalence principle. Such terms are not accounted for in our analysis.

We now compare the hybrid results for the drag coefficient of a circular cylindrical body for which $d_f = 1$ and $z = \varepsilon$. In Fig. 6(a) we plot the hybrid drag coefficient C_D versus ε , given by (84) with $d_f = 1$. In this figure we compare our hybrid results with Kaplun's three-term expansion (76), with full numerical results computed directly from (65) (see Kropinski et al. (1995)), and the experimental results of Tritton (1959). We observe

that the hybrid method provides a significantly better determination of C_D over the range $0.50 < \varepsilon < 2.0$ than does the three-term expansion (76).

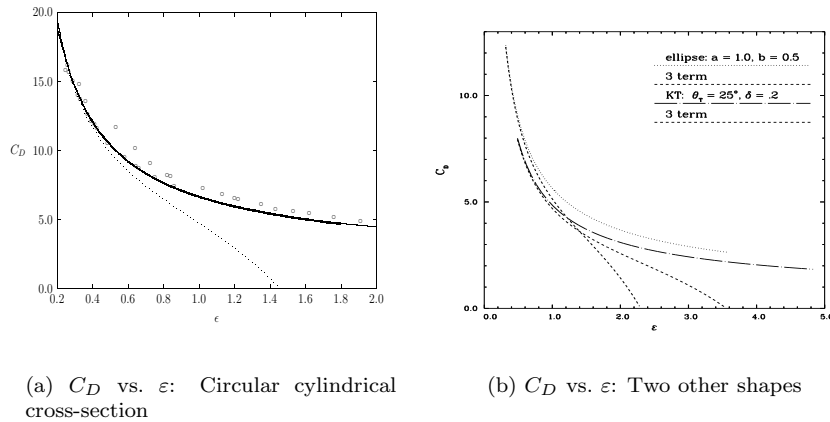


Figure 6. The drag coefficient C_D versus the Reynolds number ε . Left figure: for a circular cylinder the hybrid result (84) (solid curve), the full numerical results (heavy solid curve), the three-term result (76) (dotted curve), and the experimental results of Tritton (1959) (discrete points), are compared. Right figure: the hybrid result (84) is compared with the three-term result (76) for a cylindrical body of either an elliptical or a KT airfoil cross-section.

Finally, we consider flow around other cylindrical bodies. In Fig. 6(b) we plot the hybrid drag coefficient for flow around certain cylinders having either elliptical or KT airfoil cross-sections. In this figure, we compare, for an ellipse and an airfoil, the hybrid results for C_D with Kaplun's three-term asymptotic result (76). These results were obtained from (83) and (84), and by using the data from the plot of $R = R(S)$ in Fig. 4. The value of d_f , needed in (83), is given in (86) for the ellipse, and in Table 2 for the KT airfoil.

We now make several remarks concerning some extensions of the analysis. We first remark that our hybrid method does not incorporate the effect of the transcendentally small inertial terms arising from the Stokes region. Therefore, the asymmetry in the flow field near the body, which becomes more prominent as the Reynolds number is increased, is not captured by our

analysis. For a circular cylinder, the leading-order effects of these inertial terms on the flow field and on the drag coefficient were analyzed in Skinner (1975). In §3 of Keller and Ward (1996) an extension of the hybrid approach of Kropinski et al. (1995) was used to calculate these transcendently small terms for a circular cylinder, and to predict the asymmetry in the flow field near the body.

Secondly, we remark that a similar hybrid method was developed in Titcombe et al. (2000) to calculate the drag and lift coefficient for slow viscous flow over a cylindrical body of arbitrary cross-sectional shape. For this problem, the hybrid method solution involves a 2×2 matrix, depending on the shape of the body, which replaces the single shape-dependent parameter d_f for symmetric cylindrical bodies. In Titcombe et al. (2000) the hybrid results were compared with those of Shintani et al. (1983).

Finally, we remark that our hybrid method can also be adapted to treat some new microfluid flow problems. In Matthews and Hill (2009) (see also Matthews and Hill (2006)) the drag coefficient for steady slow viscous flow over an infinite nanocylinder was analyzed by asymptotically calculating two terms in the infinite logarithmic series for the flow field and drag coefficient. The novel feature of this microfluid flow problem is that, due to the small scales involved, the usual no-slip boundary condition on the cylinder is replaced by the Navier boundary condition, which takes into account the effect of boundary surface roughness. An analysis of this related problem by a hybrid asymptotic-numerical method will, essentially, only require the modification of the boundary condition in (68b).

4.1 Summing Logarithmic Expansions: A Linear Biharmonic Problem

In this subsection we consider a linear Biharmonic problem on a concentric annular domain with a small inner radius ε , formulated as

$$\Delta^2 u = 0, \quad \varepsilon < r < 1, \quad (88a)$$

$$u = \sin \theta, \quad u_r = 0, \quad \text{on } r = 1, \quad (88b)$$

$$u = u_r = 0, \quad \text{on } r = \varepsilon. \quad (88c)$$

We will calculate the exact solution to this problem, and then show how a hybrid method similar to that used for the low Reynolds number flow problem can be readily formulated and implemented to calculate an approximate solution to (88) that contains all logarithmic correction terms.

The exact solution of (88a), which satisfies (88b), is

$$u = \left(Ar^3 + Br \log r + \left(-2A + \frac{1}{2} - \frac{B}{2} \right) r + \left(\frac{1}{2} + A + \frac{B}{2} \right) \frac{1}{r} \right) \sin \theta, \quad (89)$$

for any constants A and B . Then, imposing that $u = u_r = 0$ on $r = \varepsilon$, we get two equations for A and B :

$$A\varepsilon^3 + B\varepsilon \log \varepsilon + \left(-2A + \frac{1}{2} - \frac{B}{2} \right) \varepsilon + \left(\frac{1}{2} + A + \frac{B}{2} \right) \varepsilon^{-1} = 0, \quad (90a)$$

$$3A\varepsilon^2 + B + B \log \varepsilon + \left(-2A + \frac{1}{2} - \frac{B}{2} \right) - \left(\frac{1}{2} + A + \frac{B}{2} \right) \varepsilon^{-2} = 0. \quad (90b)$$

By comparing the $\mathcal{O}(\varepsilon^{-1})$ and $\mathcal{O}(\varepsilon^{-2})$ terms in (90), it follows that

$$\frac{1}{2} + A + \frac{B}{2} = \kappa\varepsilon^2, \quad (91)$$

where κ is an $\mathcal{O}(1)$ constant to be found. Substituting (91) into (90), and neglecting the higher order $A\varepsilon^3$ and $3A\varepsilon^2$ terms in (90), we obtain the approximate system

$$B \log \varepsilon + \left(-2A + \frac{1}{2} - \frac{B}{2} \right) \approx -\kappa, \quad B + B \log \varepsilon + \left(-2A + \frac{1}{2} - \frac{B}{2} \right) \approx \kappa. \quad (92)$$

By adding the two equations above to eliminate κ , we obtain that

$$B + 2B \log \varepsilon + (-4A + 1 - B) = 0. \quad (93)$$

From (93), together with $A \sim -(1+B)/2$ from (91), we obtain that

$$B \sim \frac{3\nu}{2-\nu}, \quad A = 1 - \frac{3}{2-\nu}, \quad \text{where } \nu \equiv \frac{-1}{\log [\varepsilon e^{1/2}]}. \quad (94)$$

Finally, substituting (94) into (89), we obtain that the outer solution has the asymptotics

$$u \sim \left((1 - \tilde{A})r^3 + \nu \tilde{A}r \log r + \tilde{A}r \right) \sin \theta, \quad r \gg \mathcal{O}(\varepsilon). \quad (95a)$$

where \tilde{A} is defined by

$$\tilde{A} \equiv \frac{3}{2-\nu}, \quad \nu \equiv \frac{-1}{\log [\varepsilon e^{1/2}]}. \quad (95b)$$

We remark that (95) is an infinite-order logarithmic series approximation to the exact solution. However, it does not contain transcendentially small terms of algebraic order in ε as $\varepsilon \rightarrow 0$.

Next, we show how to derive (95) by employing the hybrid formulation used in the low Reynolds number flow problem of §4. In order to sum the infinite logarithmic series we formulate a hybrid method by following (77)–(79). In the inner region, with inner variable $\rho \equiv \varepsilon^{-1}r$, we look for an inner solution in the form (see (78) and (85))

$$v(\rho, \theta) = u(\varepsilon\rho, \theta) \sim \varepsilon\nu\tilde{A}(\nu) \left(\rho \log \rho - \frac{\rho}{2} + \frac{1}{2\rho} \right) \sin \theta. \quad (96)$$

Here $\nu \equiv -1/\log[\varepsilon e^{1/2}]$ and $\tilde{A} \equiv \tilde{A}(\nu)$ is a function of ν to be found. The extra factor of ε in (96) is needed since the solution in the outer region is not algebraically large as $\varepsilon \rightarrow 0$. Now letting $\rho \rightarrow \infty$, and writing (96) in terms of the outer variable $r = \varepsilon\rho$, we obtain that the far-field form of (96) is

$$v \sim \left(\tilde{A}\nu r \log r + \tilde{A}r \right) \sin \theta. \quad (97)$$

Therefore, the approximate outer hybrid solution w_H to (88) that sums all the logarithmic terms must satisfy

$$\Delta^2 w_H = 0, \quad 0 < r < 1, \quad (98a)$$

$$w_H = \sin \theta, \quad w_{Hr} = 0, \quad \text{on } r = 1, \quad (98b)$$

$$w_H \sim \left(\tilde{A}\nu r \log r + \tilde{A}r \right) \sin \theta, \quad \text{as } r \rightarrow 0. \quad (98c)$$

The solution to (98a) and (98b) is given explicitly by

$$w_H = \left(\alpha r^3 + \beta r \log r + \left(-2\alpha + \frac{1}{2} - \frac{\beta}{2} \right) r + \left(\frac{1}{2} + \alpha + \frac{\beta}{2} \right) \frac{1}{r} \right) \sin \theta. \quad (99)$$

The condition (98c) then yields the three equations

$$\beta = \tilde{A}\nu, \quad -2\alpha + \frac{1}{2} - \frac{\beta}{2} = \tilde{A}, \quad \frac{1}{2} + \alpha + \frac{\beta}{2} = 0, \quad (100)$$

for α , β , and \tilde{A} . We solve this system to obtain

$$\beta = \tilde{A}\nu, \quad \tilde{A} = \frac{3}{2 - \nu}, \quad \alpha = 1 - \tilde{A}. \quad (101)$$

Upon substituting (101) into (99), we obtain that the resulting expression agrees exactly with the result (95) obtain from the exact solution.

4.2 A Convection-Diffusion Problem

Convection-diffusion problems in two dimensional regions with obstacles in the low Peclet number limit can be analyzed in a similar way. A recent analytical study of such problems in both the low and high Peclet number limit using a different and highly innovative approach is given in Choi et al. (2005). The following analysis is related to the work in Titcombe and Ward (1997).

Consider the steady-state convection-diffusion equation for $T(\mathbf{X})$, with $\mathbf{X} = (X_1, X_2)$ posed outside two circular disks Ω_j for $j = 1, 2$ of a common radius a , and with a center-to-center separation $2L$ between the two disks:

$$\kappa \Delta T = \mathbf{U} \cdot \nabla T, \quad \mathbf{X} \in \mathbb{R}^2 \setminus \cup_{j=1}^2 \Omega_j, \quad (102a)$$

$$T = T_j, \quad \mathbf{X} \in \partial\Omega_j, \quad j = 1, 2, \quad (102b)$$

$$T = T_\infty, \quad |\mathbf{X}| \rightarrow \infty. \quad (102c)$$

Here $\kappa > 0$ is constant, T_j for $j = 1, 2$ and T_∞ are constants, and $\mathbf{U} = \mathbf{U}(\mathbf{X})$ is a given bounded flow field with $\mathbf{U}(\mathbf{X}) \rightarrow (U_\infty, 0)$ as $|\mathbf{X}| \rightarrow \infty$, where U_∞ is constant. We introduce the dimensionless variables \mathbf{x} , $\mathbf{u}(\mathbf{x})$, and $w(\mathbf{x})$ by

$$\mathbf{x} = \mathbf{X}/\gamma, \quad T = T_\infty w, \quad \mathbf{u}(\mathbf{x}) = \mathbf{U}(\gamma\mathbf{x})/U_\infty, \quad \gamma \equiv \kappa/U_\infty. \quad (103)$$

We also define the dimensionless centers of the two circular disks by \mathbf{x}_j for $j = 1, 2$, and their constant boundary temperatures α_j for $j = 1, 2$, by

$$\mathbf{x}_j = \mathbf{X}_j/\gamma, \quad \alpha_j = w_j/T_\infty, \quad j = 1, 2. \quad (104)$$

Then, (102) transforms in dimensionless form to

$$\Delta w = \mathbf{u} \cdot \nabla w, \quad \mathbf{x} \in \mathbb{R}^2 \setminus \cup_{j=1}^2 D_{\varepsilon_j}, \quad (105a)$$

$$w = \alpha_j, \quad \mathbf{x} \in \partial D_{\varepsilon_j}, \quad j = 1, 2, \quad (105b)$$

$$w \sim 1, \quad |\mathbf{x}| \rightarrow \infty. \quad (105c)$$

Here $D_{\varepsilon_j} = \{\mathbf{x} \mid |\mathbf{x} - \mathbf{x}_j| \leq \varepsilon\}$ is the circular disk of radius ε centered at \mathbf{x}_j . The center-to-center separation is

$$|\mathbf{x}_2 - \mathbf{x}_1| = 2l\varepsilon, \quad l \equiv L/a. \quad (106)$$

The dimensionless flow has limiting behavior $\mathbf{u} \sim (1, 0)$ as $|\mathbf{x}| \rightarrow \infty$. There are two interesting limiting cases of (105), which can be analyzed.

Case 1: We assume that $l = \mathcal{O}(1)$ as $\varepsilon \rightarrow 0$, so that $|\mathbf{x}_2 - \mathbf{x}_1| = \mathcal{O}(\varepsilon)$. This is the case where the bodies are close together. It leads below to a different inner problem, not considered in §2.

We assume without loss of generality that $\mathbf{x}_1 + \mathbf{x}_2 = 0$. We then introduce the inner variables \mathbf{y} and $v(\mathbf{y})$ by

$$\mathbf{y} = \varepsilon^{-1} \mathbf{x}, \quad v(\mathbf{y}) = w(\varepsilon \mathbf{y}). \quad (107)$$

Then, we obtain that (105a) and (105b) transform to

$$\Delta_{\mathbf{y}} v = \varepsilon \mathbf{u}_0 \cdot \nabla_{\mathbf{y}} v, \quad \mathbf{y} \in \mathbb{R}^2 \setminus \cup_{j=1}^2 D_j, \quad (108a)$$

$$v = \alpha_j, \quad \mathbf{y} \in \partial D_j, \quad j = 1, 2. \quad (108b)$$

Here $D_j = \{\mathbf{y} \mid |\mathbf{y} - \mathbf{y}_j| \leq 1\}$ is the circular disk centered at $\mathbf{y}_j = \mathbf{x}_j/\varepsilon$ of radius one, and $\mathbf{u}_0 \equiv \mathbf{u}(0)$. The inter-disk separation is

$$|\mathbf{y}_2 - \mathbf{y}_1| = 2l. \quad (109)$$

We then look for a solution to (108) in the form

$$v = v_0 + \nu A v_c, \quad (110)$$

where $\nu = \mathcal{O}(-1/\log \varepsilon)$ and $A = A(\nu)$ is to be found. Here v_0 solves

$$\Delta_{\mathbf{y}} v_0 = 0, \quad \mathbf{y} \in \mathbb{R}^2 \setminus \cup_{j=1}^2 D_j, \quad (111a)$$

$$v_0 = \alpha_j, \quad \mathbf{y} \in \partial D_j, \quad j = 1, 2, \quad (111b)$$

$$v_0 \text{ bounded as } |\mathbf{y}| \rightarrow \infty. \quad (111c)$$

Moreover, $v_c(\mathbf{y})$ is the solution to

$$\Delta_{\mathbf{y}} v_c = 0, \quad \mathbf{y} \in \mathbb{R}^2 \setminus \cup_{j=1}^2 D_j, \quad (112a)$$

$$v_c = 0, \quad \mathbf{y} \in \partial D_j, \quad j = 1, 2, \quad (112b)$$

$$v_c \sim \log |\mathbf{y}|, \quad \text{as } |\mathbf{y}| \rightarrow \infty. \quad (112c)$$

Since D_j for $j = 1, 2$ are non-overlapping circular disks, the problem (111) can be solved explicitly using conformal mapping and the introduction of symmetric points. In this way, we can derive that

$$v_0 \sim v_{0\infty} + o(1), \quad \text{as } |\mathbf{y}| \rightarrow \infty. \quad (113)$$

The simple calculation of $v_{0\infty}$ is omitted. When $\alpha_1 = \alpha_2 = \alpha_c$, then clearly $v_{0\infty} = \alpha_1$. Next, we can solve (112) exactly by introducing bipolar coordinates as in Appendix B of Coombs et al. (2009). In this way, we calculate that

$$v_c(\mathbf{y}) \sim \log |\mathbf{y}| - \log d + o(1), \quad |\mathbf{y}| \rightarrow \infty, \quad (114)$$

where d is given by

$$\log d = \log(2\beta) - \frac{\xi_c}{2} + \sum_{m=1}^{\infty} \frac{e^{-m\xi_c}}{m \cosh(m\xi_c)}. \quad (115)$$

Here β and ξ_c are determined in terms of l by

$$\beta = \sqrt{l^2 - 1}; \quad \xi_c = \log \left[l + \sqrt{l^2 - 1} \right]. \quad (116)$$

We remark that in this analysis we have neglected the transcendently small $\mathcal{O}(\varepsilon)$ term in (108), representing a weak drift in the inner region.

Upon substituting (113) and (114) into (110), and writing $\mathbf{y} = \varepsilon^{-1}\mathbf{x}$, we obtain in terms of outer variables that the far-field behavior of v is

$$v \sim v_{0\infty} + A + \nu A \log |\mathbf{x}|, \quad \nu \equiv \frac{-1}{\log(\varepsilon d)}. \quad (117)$$

The behavior (117) is the singularity behavior for the infinite-logarithmic series approximation $V_0(\mathbf{x}; \mu)$ to the outer solution as $\mathbf{x} \rightarrow 0$. This approximation satisfies

$$\Delta V_0 = \mathbf{u} \cdot \nabla V_0, \quad \mathbf{x} \in \mathbb{R}^2 \setminus \{0\}; \quad V_0 \sim 1, \quad |\mathbf{x}| \rightarrow \infty, \quad (118)$$

with singularity behavior (117) as $\mathbf{x} \rightarrow 0$. To solve (118), we introduce the Green's function $G(\mathbf{x}; \boldsymbol{\xi})$ satisfying

$$\Delta G = \mathbf{u} \cdot \nabla G - \delta(\mathbf{x} - \boldsymbol{\xi}), \quad \mathbf{x} \in \mathbb{R}^2, \quad (119a)$$

$$G(\mathbf{x}; \boldsymbol{\xi}) \sim -\frac{1}{2\pi} \log |\mathbf{x} - \boldsymbol{\xi}| + R(\boldsymbol{\xi}; \boldsymbol{\xi}) + o(1), \quad \mathbf{x} \rightarrow \boldsymbol{\xi}, \quad (119b)$$

with $G(\mathbf{x}; \boldsymbol{\xi}) \rightarrow 0$ as $|\mathbf{x}| \rightarrow \infty$. Here $R(\boldsymbol{\xi}; \boldsymbol{\xi})$ is the regular part of this Green's function at $\mathbf{x} = \boldsymbol{\xi}$.

The solution to (118) with singular behavior $V_0 \sim \nu A \log |\mathbf{x}|$ as $\mathbf{x} \rightarrow 0$ is

$$V_0 = 1 - 2\pi\nu A G(\mathbf{x}; 0). \quad (120)$$

By expanding (120) as $\mathbf{x} \rightarrow 0$, and equating the regular part of the resulting expression with that in (117), we get $1 - 2\pi\nu A R_{00} = A + v_{0\infty}$. This determines $A = A(\nu)$ by

$$A = \frac{1 - v_{0\infty}}{1 + 2\pi\nu R_{00}}, \quad \nu \equiv \frac{-1}{\log(\varepsilon d)}, \quad (121)$$

where $R_{00} \equiv R(0; 0)$. The outer and inner solutions are then given in terms of A . Finally, one can calculate the Nusselt number, representing

the average heat flux across the bodies, by using the divergence theorem together with the form (117) of the far-field behavior in the inner region. We leave this simple calculation to the reader.

Case 2: We assume that $l = \mathcal{O}(\varepsilon^{-1})$ as $\varepsilon \rightarrow 0$, and define $l = l_0/\varepsilon$ with $l_0 = \mathcal{O}(1)$, so that $|\mathbf{x}_2 - \mathbf{x}_1| = 2l_0$. This is the case where the small disks of radius ε are separated by $\mathcal{O}(1)$ distances in (105). In the analysis there are two distinct inner regions; one near \mathbf{x}_1 and the other at an $\mathcal{O}(1)$ distance away centered at \mathbf{x}_2 . Since each separated disk is a circle of radius ε , it has a logarithmic capacitance $d = 1$. Therefore, the infinite-logarithmic series approximation $V_0(\mathbf{x}; \mu)$ to the outer solution satisfies

$$\Delta V_0 = \mathbf{u} \cdot \nabla V_0, \quad \mathbf{x} \in \mathbb{R}^2 \setminus \{0\}; \quad V_0 \sim 1, \quad |\mathbf{x}| \rightarrow \infty, \quad (122a)$$

$$V_0 \sim \alpha_j + A_j + \nu A_j \log |\mathbf{x} - \mathbf{x}_j|, \quad \nu \equiv \frac{-1}{\log \varepsilon}. \quad (122b)$$

The solution to (122) is given explicitly by

$$V_0 = 1 - 2\pi\nu \sum_{i=1}^2 A_i G(\mathbf{x}; \mathbf{x}_i). \quad (123)$$

We then let $\mathbf{x} \rightarrow \mathbf{x}_j$ for $j = 1, 2$ in (123) and equate the nonsingular part of the resulting expression with the regular part of the singularity structure in (122b). This yields that A_1 and A_2 satisfy the linear algebraic system

$$A_1 (1 + 2\pi\nu R_{11}) + 2\pi\nu A_2 G_{12} = 1 - \alpha_1, \quad (124)$$

$$A_2 (1 + 2\pi\nu R_{22}) + 2\pi\nu A_1 G_{21} = 1 - \alpha_2. \quad (125)$$

Here $G_{ij} = G(\mathbf{x}_j; \mathbf{x}_i)$ and $R_{jj} = R(\mathbf{x}_j; \mathbf{x}_j)$ are the Green's function and its regular part as defined by (119).

Finally, we remark that for the case of a uniform flow where $\mathbf{u} = (1, 0)$, then the explicit solution to (119) is

$$G(\mathbf{x}; \boldsymbol{\xi}) = \frac{1}{2\pi} \exp \left[\frac{x_1 - \xi_1}{2} \right] K_0 (|\mathbf{x} - \boldsymbol{\xi}|), \quad (126a)$$

where $\mathbf{x} = (x_1, x_2)$ and $\boldsymbol{\xi} = (\xi_1, \xi_2)$. By letting $\mathbf{x} \rightarrow \boldsymbol{\xi}$, and using $K_0(r) \sim -\log r + \log 2 - \gamma_e$, as $r \rightarrow 0^+$, where γ_e is Euler's constant, we readily calculate that

$$R(\boldsymbol{\xi}, \boldsymbol{\xi}) = \frac{1}{2\pi} (\log 2 - \gamma_e). \quad (126b)$$

These results for G and its regular part can be used in the results of either (121) or (125) for Case I or Case II, respectively.

5 The Fundamental Neumann Eigenvalue in a Planar Domain with Localized Traps

In this section we follow Kolokolnikov et al. (2005) and consider an optimization problem for the fundamental eigenvalue of the Laplacian in a planar bounded two-dimensional domain with a reflecting boundary that is perturbed by the presence of K small holes in the interior of the domain. The perturbed eigenvalue problem is

$$\Delta u + \lambda u = 0, \quad \mathbf{x} \in \Omega \setminus \Omega_p; \quad \int_{\Omega \setminus \Omega_p} u^2 d\mathbf{x} = 1, \quad (127a)$$

$$\partial_n u = 0, \quad \mathbf{x} \in \partial\Omega; \quad u = 0, \quad \mathbf{x} \in \partial\Omega_p \equiv \cup_{i=1}^K \partial\Omega_{\varepsilon_i}. \quad (127b)$$

Here Ω is the unperturbed domain, $\Omega_p = \cup_{i=1}^K \Omega_{\varepsilon_i}$ is a collection of K small interior holes Ω_{ε_i} , for $i = 1, \dots, K$, each of ‘radius’ $\mathcal{O}(\varepsilon)$, and $\partial_n u$ is the outward normal derivative of u on $\partial\Omega$. We assume that the small holes in Ω are non-overlapping and that $\Omega_{\varepsilon_i} \rightarrow \mathbf{x}_i$ as $\varepsilon \rightarrow 0$, for $i = 1, \dots, K$. A schematic plot of the domain is shown in Fig. 7.

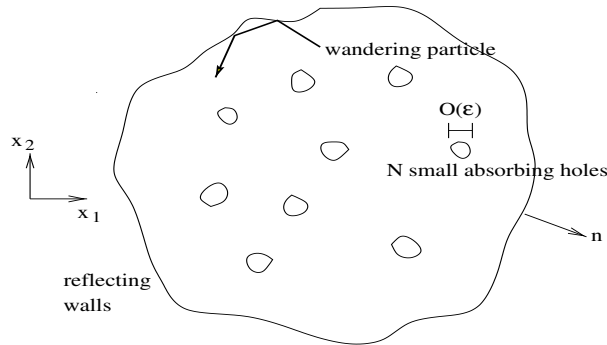


Figure 7. A schematic plot of the perturbed domain for the eigenvalue problem (127).

We let $\lambda_0(\varepsilon)$ denote the first eigenvalue of (127), with corresponding eigenfunction $u(\mathbf{x}, \varepsilon)$. Clearly, $\lambda_0(\varepsilon) \rightarrow 0$ as $\varepsilon \rightarrow 0$. Our objective is to determine the locations, \mathbf{x}_i for $i = 1, \dots, K$, of the K holes of a given shape that maximize this fundamental eigenvalue. Asymptotic expansions for the fundamental eigenvalue of related eigenvalue problems in perforated multi-dimensional domains, with various boundary conditions on the

holes and outer boundary, are given in Ozawa (1981), Ward et al. (1993), Ward and Keller (1993), Davis and Llewellyn-Smith (2007), and Lange and Weinitschke (1994) (see also the references therein).

As an application of (127), consider the Brownian motion of a particle in a two-dimensional domain Ω , with reflecting walls, that contains K small traps Ω_{ε_i} , for $i = 1, \dots, K$, each of ‘radius’ ε , for $i = 1, \dots, K$. The traps are centered at \mathbf{x}_i , for $i = 1, \dots, K$. If the Brownian particle starts from the point $\mathbf{y} \in \Omega \setminus \Omega_p$ at time $t = 0$, then the probability density $v(\mathbf{x}, \mathbf{y}, t, \varepsilon)$ that the particle is at point \mathbf{x} at time t satisfies

$$v_t = \Delta v, \quad \mathbf{x} \in \Omega \setminus \Omega_p; \quad \partial_n v = 0, \quad \mathbf{x} \in \partial\Omega; \quad v = 0, \quad \mathbf{x} \in \partial\Omega_p, \quad (128)$$

with $v = \delta(\mathbf{x} - \mathbf{y})$ at time $t = 0$. By calculating the solution to (128) in terms of an eigenfunction expansion, and by assuming that \mathbf{y} is uniformly distributed over $\Omega \setminus \Omega_p$, it is easy to show that the probability $P_0(t, \varepsilon)$ that the Brownian particle is in $\Omega \setminus \Omega_p$ at time t is given by

$$P_0(t, \varepsilon) = e^{-\lambda_0(\varepsilon)t} [1 + \mathcal{O}(\nu)]. \quad (129)$$

Therefore, the expected lifetime of the Brownian particle is proportional to $1/\lambda_0(\varepsilon)$. In this context, our optimization problem is equivalent to choosing the locations of K small traps to minimize this expected lifetime.

We first consider (127) for the case of one hole. In Ward et al. (1993) (see also Ward and Keller (1993)) it was shown that as $\varepsilon \rightarrow 0$ the first eigenvalue λ_0 of (127) has the asymptotic expansion:

$$\lambda_0(\varepsilon) = \lambda_{00} + \nu(\varepsilon)\lambda_{01} + \nu^2(\varepsilon)\lambda_{02} + \dots$$

Here, $\nu(\varepsilon) = -1/\log(\varepsilon d)$ where d is the logarithmic capacitance of the hole. For the unperturbed problem with $\varepsilon = 0$, we have $\lambda_{00} = 0$. In the $\mathcal{O}(\nu)$ term, λ_{01} is independent of the location of the hole at $\mathbf{x} = \mathbf{x}_0$ (cf. Ward et al. (1993)). Therefore, we need the higher-order coefficient λ_{02} in order to determine the location of the hole that maximizes λ_0 .

For the case of one hole, an infinite logarithmic expansion for $\lambda_0(\varepsilon)$ has the form

$$\lambda_0(\varepsilon) = \lambda^*(\nu) + \mathcal{O}\left(\frac{\varepsilon}{\log \varepsilon}\right), \quad \nu \equiv -\frac{1}{\log(\varepsilon d)}.$$

To calculate $\lambda^*(\nu)$ we use the hybrid method of Kolokolnikov et al. (2005). Near the hole, we identify an inner (local) region in terms of a local spatial variable $\mathbf{y} = \varepsilon^{-1}(\mathbf{x} - \mathbf{x}_0)$, and where the hole is rescaled so that $\Omega_0 \equiv \varepsilon^{-1}\Omega_\varepsilon$. Denoting the inner (local) solution by $v(\mathbf{y}, \varepsilon) = u(\mathbf{x}_0 + \varepsilon\mathbf{y}, \varepsilon)$, we then expand $v(\mathbf{y}, \varepsilon)$ as

$$v(\mathbf{y}, \varepsilon) = A\nu v_c(\mathbf{y}) + \dots \quad (130)$$

Here, $A = A(\nu) \sim \mathcal{O}(1)$ as $\varepsilon \rightarrow 0$, and $v_c(\mathbf{y})$ is the solution of the canonical inner problem (7), re-written here as

$$\Delta_{\mathbf{y}} v_c = 0, \quad \mathbf{y} \notin \Omega_0; \quad v_c = 0, \quad \mathbf{y} \in \partial\Omega_0, \quad (131a)$$

$$v_c \sim \log |\mathbf{y}| - \log d + \frac{\mathbf{p} \cdot \mathbf{y}}{|\mathbf{y}|^2}, \quad \text{as } |\mathbf{y}| \rightarrow \infty. \quad (131b)$$

In (131b), the logarithmic capacitance d and the dipole vector $\mathbf{p} = (p_1, p_2)$ are determined from the shape of the hole.

We expand the eigenvalue λ_0 and the outer (global) solution as

$$\lambda_0(\varepsilon) = \lambda^*(\nu) + \mu\lambda_1 + \dots, \quad u(\mathbf{x}, \varepsilon) = u^*(\mathbf{x}, \nu) + \mu u_1(\mathbf{x}, \nu) + \dots, \quad (132)$$

where $\mu \ll \mathcal{O}(\nu^k)$ for any $k > 0$. Substituting (132) into (127a) and the boundary condition (127b) on $\partial\Omega$, we obtain the full problem in a domain punctured by the point \mathbf{x}_0 ,

$$\Delta u^* + \lambda^* u^* = 0, \quad x \in \Omega \setminus \{\mathbf{x}_0\}; \quad \int_{\Omega} (u^*)^2 d\mathbf{x} = 1; \quad \partial_n u^* = 0, \quad \mathbf{x} \in \partial\Omega. \quad (133)$$

The singularity condition for (133) as $\mathbf{x} \rightarrow \mathbf{x}_0$ given below arises from matching u^* to the inner solution. Substituting (131b) into (130), and expressing the result in global variables, we obtain

$$v(\mathbf{y}, \varepsilon) \sim A\nu \log |\mathbf{x} - \mathbf{x}_0| + A + \varepsilon A\nu \frac{\mathbf{p} \cdot (\mathbf{x} - \mathbf{x}_0)}{|\mathbf{x} - \mathbf{x}_0|^2} + \dots, \quad \text{as } \mathbf{y} \rightarrow \infty. \quad (134)$$

Here, we have used $\nu \equiv -1/\log(\varepsilon d)$. To match u^* to (134), we require that u^* has the singularity behavior

$$u^*(\mathbf{x}, \nu) \sim A\nu \log |\mathbf{x} - \mathbf{x}_0| + A, \quad \text{as } \mathbf{x} \rightarrow \mathbf{x}_0. \quad (135)$$

Comparing the terms in (134) and (132) at the next order, we see that $\mu = \mathcal{O}(\varepsilon\nu)$.

Next, we must determine $u^*(\mathbf{x}, \nu)$ and $\lambda^*(\nu)$ satisfying (133) and (135). To do so, we introduce the Helmholtz Green's function, $G_h(\mathbf{x}; \mathbf{x}_0, \lambda^*)$, and its regular part, $R_h(\mathbf{x}_0; \mathbf{x}_0, \lambda^*)$, satisfying

$$\Delta G_h + \lambda^* G_h = -\delta(\mathbf{x} - \mathbf{x}_0), \quad \mathbf{x} \in \Omega; \quad \partial_n G_h = 0, \quad \mathbf{x} \in \partial\Omega, \quad (136a)$$

$$G_h(\mathbf{x}; \mathbf{x}_0, \lambda^*) \sim -\frac{1}{2\pi} \log |\mathbf{x} - \mathbf{x}_0| + R_h(\mathbf{x}_0; \mathbf{x}_0, \lambda^*) + o(1), \quad \text{as } \mathbf{x} \rightarrow \mathbf{x}_0. \quad (136b)$$

In terms of this Green's function, $u^*(\mathbf{x}, \nu)$ is given by

$$u^*(\mathbf{x}, \nu) = -2\pi A \nu G_h(\mathbf{x}; \mathbf{x}_0, \lambda^*).$$

By using (136b), we expand u^* as $\mathbf{x} \rightarrow \mathbf{x}_0$ to obtain

$$u^*(\mathbf{x}, \nu) \sim A \nu \log |\mathbf{x} - \mathbf{x}_0| - 2\pi A \nu R_h(\mathbf{x}_0; \mathbf{x}_0, \lambda^*), \quad \text{as } \mathbf{x} \rightarrow \mathbf{x}_0. \quad (137)$$

The matching condition is that the expressions in (135) and (137) agree. The $\log |\mathbf{x} - \mathbf{x}_0|$ terms agree automatically, and from the remaining terms, we obtain a transcendental equation for $\lambda^*(\nu)$ given by

$$R_h(\mathbf{x}_0; \mathbf{x}_0, \lambda^*) = -\frac{1}{2\pi\nu}. \quad (138)$$

To obtain the asymptotic behavior for λ_0 , we need the solution λ^* of (138) that tends to zero as $\nu \rightarrow 0$.

Equation (138) can, in general, only be solved numerically as a function of ν . Below, we only determine an expression for λ^* that is correct to terms of order $\mathcal{O}(\nu^2)$. To obtain this expression, we expand the Helmholtz Green's function, $G_h(\mathbf{x}; \mathbf{x}_0, \lambda^*)$, in terms of $\lambda^* \ll 1$, as

$$G(\mathbf{x}; \mathbf{x}_0, \lambda^*) = \frac{1}{\lambda^*} G_0(\mathbf{x}; \mathbf{x}_0) + G_1(\mathbf{x}; \mathbf{x}_0) + \lambda^* G_2(\mathbf{x}; \mathbf{x}_0) + \dots \quad (139)$$

Substituting (139) into (136), we get a series of problems for the $G_j(\mathbf{x}; \mathbf{x}_0)$, $j = 0, 1, 2, \dots$. At order $\mathcal{O}(1/\lambda^*)$, G_0 satisfies $\Delta G_0 = 0$ in Ω and $\partial_n G_0 = 0$ on $\partial\Omega$, from which we obtain that G_0 is a constant. The higher-order corrections G_j for $j \geq 1$ are readily found to satisfy

$$\Delta G_j = \begin{cases} -\delta(\mathbf{x} - \mathbf{x}_0) - G_0, & j = 1, \\ -G_{j-1}, & j > 1, \end{cases} \quad \mathbf{x} \in \Omega; \quad \partial_n G_j = 0, \quad \mathbf{x} \in \partial\Omega, \quad (140)$$

with $\int_{\Omega} G_j d\mathbf{x} = 0$ for $j \geq 1$. Applying the Divergence Theorem, we obtain that $G_0 = -1/|\Omega|$, where $|\Omega|$ is the area of Ω . The function $G_1(\mathbf{x}; \mathbf{x}_0)$ (which we shall henceforth call G_N) is the Neumann Green's function, with regular part $R_N(\mathbf{x}_0; \mathbf{x}_0)$ defined by (49).

From (139) and (49b), we write the two-term expansion for G when $\lambda^* \ll 1$ as

$$G_h(\mathbf{x}; \mathbf{x}_0, \lambda^*) = -\frac{1}{|\Omega|\lambda^*} + G_N(\mathbf{x}; \mathbf{x}_0) + \mathcal{O}(\lambda^*). \quad (141)$$

A similar two-term expansion for the regular part R_h of the Helmholtz Green's function in terms of the regular part of the Neumann Green's function is

$$R_h(\mathbf{x}_0; \mathbf{x}_0, \lambda^*) = -\frac{1}{|\Omega|\lambda^*} + R_N(\mathbf{x}_0; \mathbf{x}_0) + \mathcal{O}(\lambda^*). \quad (142)$$

Substituting this expression into (138), we get the following two-term asymptotic result:

Principal Result 3:(One Hole) For $\varepsilon \rightarrow 0$, the first eigenvalue λ_0 of (127) has the two-term asymptotic behavior

$$\lambda_0(\varepsilon) = \frac{2\pi\nu}{|\Omega|(1+2\pi\nu R_N(\mathbf{x}_0; \mathbf{x}_0))} + \mathcal{O}(\nu^3) = \frac{2\pi\nu}{|\Omega|} - \frac{4\pi^2\nu^2}{|\Omega|} R_N(\mathbf{x}_0; \mathbf{x}_0) + \mathcal{O}(\nu^3). \quad (143)$$

Here $\nu = -1/\log(\varepsilon d)$, and d is the logarithmic capacitance determined from the inner problem (131). An infinite-order logarithmic expansion for λ_0 is given by $\lambda_0 \sim \lambda^*$, where λ^* is the first positive root of (138).

Next, we extend the asymptotic framework to the case of K holes. Much of the analysis above remains the same, except that now the single hole \mathbf{x}_0 is replaced by \mathbf{x}_i , for $i = 1, \dots, K$. The hybrid formulation for K holes is

$$\Delta u^* + \lambda^* u^* = 0, \quad x \in \Omega \setminus \{\mathbf{x}_1, \dots, \mathbf{x}_K\}; \quad \partial_n u^* = 0, \quad \mathbf{x} \in \partial\Omega, \quad (144a)$$

$$u^* \sim A_i \nu_i \log |\mathbf{x} - \mathbf{x}_i| + A_i, \quad \text{as } \mathbf{x} \rightarrow \mathbf{x}_i, \quad i = 1, \dots, K, \quad (144b)$$

with normalization condition $\int_{\Omega} (u^*)^2 d\mathbf{x} = 1$. Here, $\nu_i = -1/\log(\varepsilon d_i)$, where d_i is the logarithmic capacitance of the i^{th} hole. In this formulation, we have the K unknowns, A_i , for $i = 1, \dots, K$, and one normalization condition for u^* . The normalization condition effectively sets one relation between the A_i , for $i = 1, \dots, K$.

We write u^* in terms of the Helmholtz Green's function defined in (136), and then take the limit $\mathbf{x} \rightarrow \mathbf{x}_i$ to get

$$u^* = -2\pi \sum_{j=1}^K A_j \nu_j G_h(\mathbf{x}; \mathbf{x}_j, \lambda^*) \sim A_i \nu_i (\log |\mathbf{x} - \mathbf{x}_i| - 2\pi \nu_i R_h(\mathbf{x}_i; \mathbf{x}_i, \lambda^*)) - 2\pi \sum_{\substack{j=1 \\ j \neq i}}^K A_j \nu_j G_h(\mathbf{x}_i; \mathbf{x}_j, \lambda^*). \quad (145)$$

The matching condition is that the expressions in (144b) and (145) agree. The logarithmic terms agree, and from the remaining terms, we obtain a $K \times K$ homogeneous linear system to solve for the A_i , given by

$$A_i (1 + 2\pi \nu_i R_h(\mathbf{x}_i; \mathbf{x}_i, \lambda^*)) + 2\pi \sum_{\substack{j=1 \\ j \neq i}}^K A_j \nu_j G_h(\mathbf{x}_i; \mathbf{x}_j, \lambda^*) = 0, \quad i = 1, \dots, K. \quad (146)$$

A solution to (146) exists only when the determinant associated with the linear system (146) vanishes. This condition provides an expression for $\lambda^*(\nu_1, \dots, \nu_K)$ that sums all the logarithmic terms in the asymptotic expansion of $\lambda_0(\varepsilon)$.

As with the case for one hole in the domain, we can derive an asymptotic formula for λ^* that has an error of $\mathcal{O}(\nu^3)$. This formula is again determined in terms of the Neumann Green's function G_N and its regular part R_N , defined in (49). By using (141) and (142) in (146), we obtain a homogeneous linear system for the A_i for $i = 1, \dots, K$, given by

$$A_i \left[1 + 2\pi\nu_i R_N(\mathbf{x}_j; \mathbf{x}_j) - \frac{2\pi\nu_i}{|\Omega|\lambda^*} \right] + 2\pi \sum_{\substack{j=1 \\ j \neq i}}^K A_j \nu_j \left[-\frac{1}{|\Omega|\lambda^*} + G_N(\mathbf{x}_j; \mathbf{x}_i) \right] = 0. \quad (147)$$

It is convenient to write (147) in matrix form as

$$\mathcal{C}\mathbf{a} = \frac{2\pi}{|\Omega|\lambda^*} \mathcal{B}\mathcal{V}\mathbf{a}, \quad \mathcal{C} \equiv I + 2\pi\mathcal{G}_N\mathcal{V}, \quad (148a)$$

where

$$\mathcal{V} \equiv \begin{pmatrix} \nu_1 & 0 & \cdots & 0 \\ 0 & \ddots & \cdots & 0 \\ \vdots & \vdots & \ddots & \vdots \\ 0 & 0 & \cdots & \nu_K \end{pmatrix}, \quad \mathcal{B} \equiv \begin{pmatrix} 1 & 1 & \cdots & 1 \\ 1 & \ddots & \cdots & 1 \\ \vdots & \vdots & \ddots & \vdots \\ 1 & 1 & \cdots & 1 \end{pmatrix}, \quad \mathbf{a} \equiv \begin{pmatrix} A_1 \\ \vdots \\ A_K \end{pmatrix}. \quad (148b)$$

In (148a), the Neumann Green's function matrix \mathcal{G}_N is the $K \times K$ symmetric matrix with entries

$$(\mathcal{G}_N)_{ij} \equiv G_N(\mathbf{x}_i; \mathbf{x}_j), \quad i \neq j; \quad (\mathcal{G}_N)_{jj} = R_N(\mathbf{x}_j; \mathbf{x}_j). \quad (148c)$$

Let $\nu_m = \max_{j=1, \dots, K} \nu_j$. Then, for ν_m sufficiently small, we can invert \mathcal{C} approximately, to obtain that λ^* is an eigenvalue of the matrix eigenvalue problem

$$\mathcal{A}\mathbf{a} = \lambda^* \mathbf{a}, \quad \mathcal{A} = \frac{2\pi}{|\Omega|} \mathcal{C}^{-1} \mathcal{B}\mathcal{V}. \quad (149)$$

By using this representation of λ^* we obtain the following result:

Principal Result 4: (K Holes) For $\varepsilon \rightarrow 0$, the first eigenvalue λ_0 of (127) has the explicit two-term asymptotic behavior

$$\lambda_0(\varepsilon) \sim \lambda^*, \quad \lambda^* = \frac{2\pi}{|\Omega|} \left(\sum_{j=1}^K \nu_j - 2\pi \sum_{j=1}^K \sum_{i=1}^K \nu_j \nu_i (\mathcal{G})_{Nij} \right) + \mathcal{O}(\nu_m^3). \quad (150)$$

Here $(\mathcal{G})_{Nij}$ are the entries of the Neumann Green's function matrix \mathcal{G}_N defined in (148c).

Proof. We first notice that the matrix $\mathcal{B}\mathcal{V}$ has rank one, since \mathcal{V} is diagonal and $\mathcal{B} = \mathbf{e}_0 \mathbf{e}_0^t$, where $\mathbf{e}_0^t = (1, 1, \dots, 1)$. This implies that \mathcal{A} has rank one, and so λ^* is the unique nonzero eigenvalue of \mathcal{A} . Hence, $\lambda^* = \text{Trace}\mathcal{A}$. By using the structure of \mathcal{A} in (149), we readily calculate that

$$\lambda^* = \frac{2\pi}{|\Omega|} \sum_{j=1}^K \nu_j \left(\sum_{i=1}^K c_{ij} \right), \quad c_{ij} \equiv (\mathcal{C}^{-1})_{ij}. \quad (151)$$

Finally, we use the asymptotic inverse $\mathcal{C}^{-1} \sim I - 2\pi\mathcal{G}_N\mathcal{V} + \dots$ for $\nu_m \ll 1$ to calculate c_{ij} . Substituting this result into (151) we obtain (150). \square

As a Corollary to this result, we obtain the following simplification for the case of K identical holes:

Corollary 5:(K Identical Holes) Suppose that the K holes are identical, in the sense that εd_j is independent of j . Then, (150) can be written as the explicit two-term expansion

$$\lambda_0(\varepsilon) \sim \lambda^*, \quad \lambda^* = \frac{2\pi K\nu}{|\Omega|} - \frac{4\pi^2\nu^2}{|\Omega|} p(\mathbf{x}_1, \dots, \mathbf{x}_K) + \mathcal{O}(\nu^3), \quad (152)$$

where $\nu \equiv -1/\log(\varepsilon d)$, and the function $p(\mathbf{x}_1, \dots, \mathbf{x}_K)$ is defined by

$$p(\mathbf{x}_1, \dots, \mathbf{x}_K) = \sum_{j=1}^K \sum_{i=1}^K (\mathcal{G})_{Nij} = \sum_{i=1}^K \left(R_N(\mathbf{x}_i; \mathbf{x}_i) + \sum_{\substack{j=1 \\ j \neq i}}^K G_N(\mathbf{x}_j; \mathbf{x}_i) \right). \quad (153)$$

Here $(\mathcal{G})_{Nij}$ are the entries in the matrix \mathcal{G}_N in (148c). For K circular holes of radius ε , then $d_j = 1$ for $j = 1, \dots, K$, and so $\nu = -1/\log \varepsilon$.

When Ω is the unit disk, the optimal spatial configurations of the centers $\{\mathbf{x}_1, \dots, \mathbf{x}_K\}$ of K distinct traps of a common radius ε were computed numerically in Kolokolnikov et al. (2005) by optimizing the function $p(\mathbf{x}_1, \dots, \mathbf{x}_K)$ in (153). For the unit disk, the Neumann Green's function $G_N(\mathbf{x}; \boldsymbol{\xi})$ and its regular part $R_N(\boldsymbol{\xi}; \boldsymbol{\xi})$ are explicitly available (see equation (52)). By using this Green's function, it is readily shown that the problem of minimizing the function $p(\mathbf{x}_1, \dots, \mathbf{x}_K)$ is equivalent to the discrete

variational problem of minimizing the function $\mathcal{F}(\mathbf{x}_1, \dots, \mathbf{x}_K)$ defined by

$$\mathcal{F}(\mathbf{x}_1, \dots, \mathbf{x}_K) = - \sum_{j=1}^K \sum_{\substack{k=1 \\ k \neq j}}^K \log |\mathbf{x}_j - \mathbf{x}_k| - \sum_{j=1}^K \sum_{k=1}^K \log |1 - \mathbf{x}_j \bar{\mathbf{x}}_k| + K \sum_{j=1}^K |\mathbf{x}_j|^2, \quad (154)$$

for $|x_{ij}| = 1$ and $\mathbf{x}_j \neq \mathbf{x}_k$ when $j \neq k$. Here $\bar{\mathbf{x}}_k$ denotes the complex conjugate of \mathbf{x}_k .

An interesting open problem is to determine the optimal arrangement of $K \gg 1$ traps in the dilute fraction limit $K\varepsilon^2 \ll 1$. In particular, does the optimal arrangement approach a hexagonal lattice structure with a boundary layer near the rim of the unit disk?

6 Conclusion

In this article we have surveyed the development and application of a hybrid asymptotic-numerical method for solving linear and nonlinear PDE models in two-dimensional domains that have small inclusions or obstructions. Related theoretical approaches have also been developed to treat similar strongly localized perturbation problems including, an eigenvalue perturbation problem in a three-dimensional domain (cf. Ward and Keller (1993)), cell-signaling problems in mathematical biology (cf. Bressloff et al. (2008), Straube and Ward (2009)), the narrow escape problem from a sphere or a disk that has small absorbing windows on its boundary (cf. Cheviakov et al. (to appear, 2010), Pillay et al. (to appear, 2010)), and the mean first passage time in a three-dimensional domain with interior traps (cf. Cheviakov and Ward (to appear, 2010)).

Acknowledgments

M. J. W. gratefully acknowledges the fundamental contributions of my other co-authors D. Coombs (UBC), J. B. Keller (Stanford), T. Kolokolnikov (Dalhousie), A. Peirce (UBC), S. Pillay (J.P. Morgan), R. Straube (Max Planck Institute, Magdeburg), and M. Titcombe (Champlain College) to some of the work surveyed herein. M. J. W. and M. C. K. acknowledge the grant support of NSERC (Canada).

Bibliography

C. Bandle and M. Flucher. Harmonic radius and concentration of energy; hyperbolic radius and liouville's equation. *SIAM Review*, 38(2):191–238,

- 1996.
- P. C. Bressloff, D. Earnshaw, and M. J. Ward. Diffusion of protein receptors on a cylindrical dendritic membrane with partially absorbing traps. *SIAM J. Appl. Math.*, 68(5):1223–1246, 2008.
- A. Cheviakov and M. J. Ward. Optimizing the fundamental eigenvalue of the laplacian in a sphere with interior traps. *Mathematical and Computer Modeling*, to appear, 2010.
- A. Cheviakov, M. J. Ward, and R. Straube. An asymptotic analysis of the mean first passage time for narrow escape problems: Part ii: The sphere. *SIAM J. Multiscale Modeling*, to appear, 2010.
- J. Choi, D. Margetis, T. M. Squires, and M. Z. Bazant. Steady advection-diffusion around finite absorbers in two-dimensional potential flows. *J. Fluid Mech.*, 536:155–184, 2005.
- D. Coombs, R. Straube, and M. J. Ward. Diffusion on a sphere with localized traps: Mean first passage time, eigenvalue asymptotics, and feketé points. *SIAM J. Appl. Math.*, 70(1):302–332, 2009.
- A. M. Davis and S. G. Llewellyn-Smith. Perturbation of eigenvalues due to gaps in two-dimensional boundaries. *Proc. Roy. Soc. A*, 463:759–786, 2007.
- W. W. Dijkstra and M. E. Hochstenbach. Numerical approximation of the logarithmic capacity. *CASA Report 08-09, Technical U. Eindhoven*, 2008.
- M. Van Dyke. *Perturbations Methods in Fluid Mechanics*. Parabolic Press, 1975.
- J. E. Fletcher. Mathematical modeling of the microcirculation. *Math Biosciences*, 38:159–202, 1978.
- I. Imai. On the asymptotic behavior of viscous fluid flow at a great distance from a cylindrical body, with special reference to filon’s paradox. *Proc. Roy. Soc. A*, 208:487–516, 1951.
- S. Kaplun. Low reynolds number flow past a circular cylinder. *J. Math. Mech.*, 6(5):52–60, 1957.
- J. B. Keller and M. J. Ward. Asymptotics beyond all orders for a low reynolds number flow. *J. Engrg. Math.*, 30(1-2):253–265, 1996.
- J. Kevorkian and J. Cole. *Multiple Scale and Singular Perturbation Methods*. Applied Mathematical Sciences, Vol. 114, Springer-Verlag, 1993.
- T. Kolokolnikov, M. Titcombe, and M. J. Ward. Optimizing the fundamental neumann eigenvalue for the laplacian in a domain with small traps. *Europ. J. Appl. Math.*, 16(2):161–200, 2005.
- A. Krogh. The number and distribution of capillaries in muscles with calculations of the oxygen pressure head necessary for supplying the tissue. *J. Physiology (London)*, 52:409–415, 1919.

- M. C. Kropinski, M. J. Ward, and J. B. Keller. A hybrid asymptotic-numerical method for calculating low reynolds number flows past symmetric cylindrical bodies. *SIAM J. Appl. Math.*, 55(6):1484–1510, 1995.
- P. A. Lagerstrom. *Matched Asymptotic Expansions*. Applied Mathematical Sciences, Vol. 76, Springer-Verlag, 1988.
- C. Lange and H. Weinitzschke. Singular perturbations of elliptic problems on domains with small holes. *Stud. Appl. Math.*, 92(1):55–93, 1994.
- S. H. Lee and L. G. Leal. Low reynolds number flow past cylindrical bodies of arbitrary cross-sectional shape. *J. Fluid Mech.*, 164:401–427, 1986.
- MATLAB. *Partial Differential Equations Toolbox, User's Guide*. The MathWorks, Inc., 1996.
- M. Matthews and J. Hill. Flow around nanospheres and nanocylinders. *Q. J. Mech. Appl. Math.*, 59(2):191–210, 2006.
- M. Matthews and J. Hill. Asymptotic analysis of the viscous micro/nano pump at low reynolds number. *J. Engrg. Math.*, 63(2-4):279–292, 2009.
- A. Mikelić and M. Primicerio. A diffusion-consumption problem for oxygen in a living tissue perfused by capillaries. *Nonlinear Diff. Eq. Appl.*, 13(3):349–367, 2006.
- L. M. Milne-Thomson. *Theoretical Aerodynamics*. Dover Publications Inc., 1958.
- S. Ozawa. Singular variation of domains and eigenvalues of the laplacian. *Duke Math. J.*, 48(4):767–778, 1981.
- S. Pillay, M. J. Ward, A. Peirce, and T. Kolokolnikov. An asymptotic analysis of the mean first passage time for narrow escape problems: Part i: Two-dimensional domains. *SIAM J. Multiscale Modeling*, to appear, 2010.
- A. S. Popel. Theory of oxygen transport to tissue. *Critical Reviews in Biomedical Engrg.*, 17:257–321, 1989.
- I. Proudman and J. Pearson. Expansions at small reynolds number for the flow past a sphere and a circular cylinder. *J. Fluid Mech.*, 2:237–262, 1957.
- K. B. Ranger. Explicit solutions of the steady two-dimensional navier-stokes equations. *Stud. Appl. Math.*, 94(2):169–181, 1995.
- T. Ransford. *Potential Theory in the Complex Plane*. London Mathematical Society Student Texts Vol. 28, Cambridge University Press, 1995.
- K. Shintani, A. Umemura, and A. Takano. Low reynolds number flow past an elliptic cylinder. *J. Fluid Mech.*, 136:277–289, 1983.
- L. A. Skinner. Generalized expansions for slow flow past a cylinder. *Q. J. Mech. Appl. Math.*, 28(3):333–340, 1975.

- R. Straube and M. J. Ward. Intracellular signalling gradients arising from multiple compartments: A matched asymptotic expansion approach. *SIAM J. Appl. Math.*, 70(1):248–269, 2009.
- M. Titcombe and M. J. Ward. Convective heat transfer past small cylindrical bodies. *Stud. Appl. Math.*, 99(1):81–105, 1997.
- M. Titcombe and M. J. Ward. Summing logarithmic expansions for elliptic equations in multiply-connected domains with small holes. *Canadian Appl. Math. Quart.*, 7(3):313–343, 1999.
- M. Titcombe and M. J. Ward. An asymptotic study of oxygen transport from multiple capillaries to skeletal muscle tissue. *SIAM J. Appl. Math.*, 60(5):1767–1788, 2000.
- M. Titcombe, M. J. Ward, and M. C. Kropinski. A hybrid asymptotic-numerical solution for low reynolds number flow past an asymmetric cylindrical body. *Stud. Appl. Math.*, 105(2):165–190, 2000.
- D. J. Tritton. Experiments on the flow past a circular cylinder at low reynolds numbers. *J. Fluid Mech.*, 6:547–567, 1959.
- J. Veysey and N. Goldenfeld. Simple viscous flows: From boundary layers to the renormalization group. *Reviews of Modern Physics*, 79:883–927, 2007.
- M. J. Ward, W. D. Henshaw, and J. B. Keller. Summing logarithmic expansions for singularly perturbed eigenvalue problems. *SIAM J. Appl. Math.*, 53(3):799–828, 1993.
- M. J. Ward and J. B. Keller. Strong localized perturbations of eigenvalue problems. *SIAM J. Appl. Math.*, 53(3):770–798, 1993.
- A. J. Ward-Smith. *Internal Fluid Flow*. Clarendon Press, Oxford, 1980.